Laporan Akhir Projek Penyelidikan Jangka Pendek

Development of Nanostructured Iron Oxide Colloid Augmented Polymeric Membrane To Remove Arsenic From Drinking Water For The Bottom Billion

By
Assoc. Prof. Dr. Lim Jit Kang

2014

UNIVERSITI SAINS MALAYSIA

Pusat Pengajian
Kejuruteraan Kimia
School of
Chemical Engineering

Kampus Kejuruteraan
Universiti Sains Malaysia
Seri Ampangan,
14300 Nibong Tebal,
Seberang Perai Selatan,
Pulau Pinang, Malaysia.
Telefon 604 599 5999 samb. 6401/6407
Facsimile 604 594 1013
http://chemical.eng.usm.my

12 Januari 2015

Encik Abdul Hafiz Abdul Hadi
Penolong Pendaftar
Unit Pengurusan Geran Dan Pembangunan Penyelidikan
Bahagian Penyelidikan Dan Inovasi
Universiti Sains Malaysia
11800
Pulau Pinang

Tuan

Laporan Akhir Projek Penyelidikan Tajaan International Foundation for Science (IFS)

Tajuk Projek: **Development of Nanostructured Iron Oxide Colloid Augmented Polymeric Membrane to Remove Arsenic from Drinking Water for the Bottom Billion**
Ketua Projek: **Prof. Madya Dr. Lim Jit Kang**
No. Akuan: **304/PJKIMIA/6050232/I100**

Dengan segala hormatnya, perkara di atas adalah berkaitan dan dirujuk.

2. Sehubungan dengan itu, sukacita disertakan bersama-sama ini Laporan Akhir bagi projek penyelidikan IFS untuk saya yang telah dilengkapi dengan salinan kertas kerja penyelidikan. Sebenarnya, laporan akhir ini telah diserahkan kepada pejabat tuan dan juga penaja geran IFS pada bulan Oktober 2014. Sila rujuk lampiran untuk emel diantara pihak IFS dengan saya.

Sekian, untuk tindakan pihak tuan yang selanjutnya. Terima Kasih

"BERKHIDMAT UNTUK NEGARA"
'Memastikan Kelestarian Hari Esok'

(Prof. Madya Dr. Lim Jit Kang) x6423
Pusat Pengajian Kejuruteraan Kimia

Tutup Geran.

PROF. DR LEE KEAT TEONG
Pengarah
Pejabat Pengurusan & Kreativiti Penyelidikan
Universiti Sains Malaysia
11800 USM, Pulau Pinang.

E: IFS grant final report W/5098-1

:va Rostig <eva.rostig@ifs.se>

ri 10/24/2014 3:58 PM

Lim Jit Kang <chjitkangl@usm.my>;

1 attachment

JIDELINES FOR REPORTS AND EXPENDITURES FORM.doc;

ear Dr JitKang,

any thanks for your message with the renewal application, Report and 1st page signed. When your application has one through the pre-screening phase we will let you know. I would also need you to send us the Statement of (penditures attached to the Guidelines on how to present your Report duly filled in and signed. In case you do not ave the Guidelines any longer I attached a copy.

est wishes from Stockholm

'va Rostig
rogram Administrator
latural Products Area
ıternational Foundation for Science (IFS)
:arlavägen 108, 5th floor
;E-115 26 Stockholm, Sweden
'hone: +46-8-545 818 08; E-mail: Eva.Rostig@ifs.se; Web: www.ifs.se

---

'rom: Lim Jit Kang [mailto:chjitkangl@usm.my]
Sent: den 24 oktober 2014 05:03
To: Eva Rostig
Subject: IFS grant final report W/5098-1

Hi Eva,
Please find attached:

1. Final report for my first IFS grant W/5098-1(all in one PDF)
2. My 2nd IFS proposal
3. Signed first page of my 2nd IFS proposal

Please kindly acknowledge the receipt of this email. Your coordination efforts on this matter is greatly appreciated.

Thanks, JitKang

)m: Eva Rostig <eva.rostig@ifs.se>
nt: Wednesday, October 1, 2014 5:52 PM
: Lim Jit Kang
bject: RE: IFS grant final report W/5098-1

ar JitKang,

ıst discovered that I opened your message but forgot to respond to the same. Terribly sorry for this. Attached you l find the Guidelines for how to write your Report.

you have had the total of your grant transferred to your Institution, you also need to fill in and return the :ached Expenditures form.

ould you wish to re-apply for your second and final grant, you may do so even if Malaysia no longer is an eligible untry for IFS. I attach for that purpose the appropriate form. You should send all the documents directly to me.

st wishes from a sunny Stockholm..... Eva

'a Rostig
ɔgram Administrator
ıtural Products Area
ernational Foundation for Science (IFS)
ırlavägen 108, 5th floor
:-115 26 Stockholm, Sweden
ıone: +46-8-545 818 08; E-mail: Eva.Rostig@ifs.se; Web: www.ifs.se

---

om: Lim Jit Kang [mailto:chjitkangl@usm.my]
ınt: den 27 juni 2014 07:07
ı: Eva Rostig
ıbject: IFS grant final report W/5098-1

Eva,
This is JitKang Lim from Universiti Sains Malaysia. Currently, I am writing up my final report for IFS ant (W/5098-1) and am wondering what is the format I should be using? I can't find anything online ɔout the format of the final report. Your insight on this matter is greatly appreciated.

ıanks, JitKang

Grantee W/5098-1

Development of Nanostructured Iron Oxide Colloid Augmented Polymeric Membrane To Remove Arsenic/Heavy Metal From Drinking Water For The Bottom Billion

April 01, 2012 – Sept 30, 2014 (30 months)

JitKang Lim, School of Chemical Engineering, Engineering Campus, Universiti Sains Malaysia, Seri Ampangan, 14300 Nibong Tebal, Pulau Pinang, Malaysia.

Summary

In this study the synthesis and applications of magnetic nanoparticles augmented polymeric structures, such as microcapsules and flat sheet membrane, for the removal of heavy metal from water resources was described in detail. Combinations of these two structures, namely nanoparticles and polymeric network, into single entity further enhance the pollutant removal efficiency as it capable to remove targeted pollutant through two mechanisms: entrapment by polymeric network, follow by adsorption and catalytic reduction (Fenton reaction) by nanoparticles. Whereas having magnetic response enables the recollection, hence recycling, of the microcapsule by magnetophoresis. This study will focus on to understand how the colloidal based interfacial effects, such as surface functionalization of the nanoparticles, colloid stability, surface-to-volume ratio, contribute toward the combinatorial advantages of nanoparticles augmented polymeric microcapsule for pollutant removal. A model system by using arsenic and other heavy metals (especially those can be found in semiconductor industry waste water) as targeted pollutant will be employed to test the feasibility of this idea. Since, the principle investigate is currently pursuing his research career in the northern state of Malaysia, Penang, where most of the semiconductor factories in the country are currently located, hence, the model system chosen is highly relevant to the local community.

1. Introduction

In recent years magnetic nanoparticles (NPs) with sizes ranging from 1 to 100 nm have attracted much interest in many environmental engineering related applications mainly due to its ability to serve as nanosorbents [1] for pollutant removal from water resources [2]. Nano-sized particles with high surface-to-volume ratio, and hence, high loading capacity, has making it an ideal candidate as nanoagent to remove pollutants such as trichloroethylene (TCE) [3], arsenic [4] and heavy metals [5], organic waste [6] and dye [7] out from water resources. As for the realization of engineering applications of the magnetic NPs is concerned, the strong adsorptive behaviour of arsenic and heavy metal onto iron oxide nanocrystalline surface [8], together with their catalytic [6] and magnetic [2] properties, placed them in an advantageous position to remove these compounds contaminated water.

To benefit from the aforementioned unique features of magnetic NPs for pollutants removal from water resources, most of the strategy proposed to date, such as the one suggested by Saha and coworkers [8], are relying on the initial exposure of pollutant to freely suspended NPs follows with the recollection of the particles by an externally applied magnetic field. Since the magnetophoretic forces experienced by the NPs are proportional to their volume (see Eq. 1) [9], hence, the re-collection of the freely suspended nanoparticles is extremely difficult as ultra-large magnetic field gradient ∇B is required to generate high F_{mag} to overcome the thermal randomization energy originated from the Brownian motion of the particles [10]. This limitation makes direct collection of NPs less attractive.

$$F_{mag} = \frac{V_m \Delta\chi}{\mu_0}(B \cdot \nabla)B \qquad \text{(Eq. 1)}$$

In addition, more evidences have recently surfaced indicating the risk of (eco)toxicological impacts of nanomaterials [11]. The contributing factors of nanotoxicity are still subjected to debate; however, it is very likely due to the characteristic small dimensional effects of nanomaterials that are not shared by its non-nanoscale counterparts with the same chemical composition [12], or, biophysicochemical interations at the nano-bio interface dictated by colloidal forces [13]. For either reason, the release of great amount of NPs without surface functionalization to environment should be avoided.

In the present study, we propose the usage of magnetic NPs-polymeric microcapsule for arsenic and heavy metal removal from water resources. The encapsulation of the NPs within polymeric network would drastically reduce the risk associated to the nanotoxicity as the direct physical contact of the NPs to its surrounding is minimal. In addition, the polymeric matrix acts as a barrier to localize the magnetic nanoparticles (acting as a catalyst) and pollutants in confined space, which subsequently would improve their physical contact and promote the catalytic degradation of pollutants [14]. Furthermore, the microcapsules prepared would also exhibit better catalytic stability and recyclability without loss of activity after multiple cycles of catalytic degradation runs [15]. Due to the collective magnetophoretic forces experienced by all the trapped NPs, we anticipated that this hybrid material would response much rapidly even at very low magnetic field gradient compared to individual particle. Two commercially available Fe^0/iron oxides nanorods from TODA America and nanosphere from Sigma Aldrich (Fig. 1) were encapsulated into three dimensional polyvinilydene fluoride (PVDF) polymeric networks to form microcapsule by using phase inversion technique (Fig. 1) [16]. We used these two species of magnetic nanoparticles because of their differences in (i) magnetophoretic behaviour [10,17],

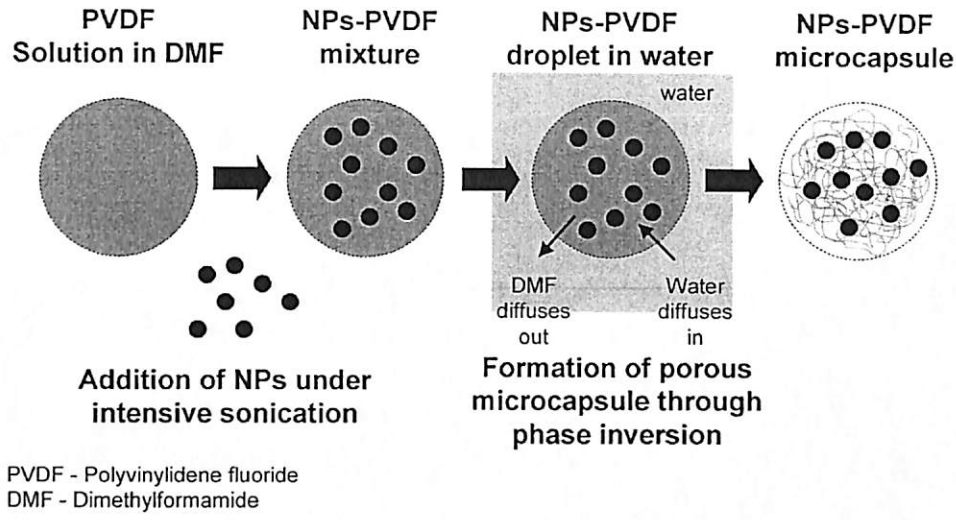

Figure 1. Pictorial representation showing the steps involved in phase inversion technique to synthesize magnetic nanoparticles augmented PVDF microcapsule.

(ii) dispersibility of the particle suspension formed as rod-like magnetic nanoparticles has higher tendency to aggregate than spherical particles, so, the colloidal stability effects on MB removal can be tested, and also (iii) their availability in large quantity which is crucial for the engineering applications of nanomaterials. Whereas PVDF is used as base polymer for the construction of microcapsule due to advantages such as high purity, high mechanical strength and its high chemical, pH and heat resistance [18].

2. Materials and Methods

2.1. Materials

Polyvinylidene fluoride (PVDF) was purchased from Solef, Solvay Solexis. Dimethylformamide (DMF), hydrogen peroxide (35 wt.% in water) and Methylene blue (MB) (M_w=319.8) was obtained from Merck. The Fe^0/iron oxides nanosphere (with hydrodynamic diameter ~20 nm) and nanorods (with length ~300 nm and diameter ~20 nm) [17] were

supplied by Sigma Aldrich and TODA America, respectively (Fig.1). Alternating gradient magnetometry [17] and vibrating sample magnetometry (conducted by ARkival Technology Corp., USA) measurements were performed at room temperature on a know amount of TODA nanorod and Sigma nanospheres and the specific magnetization of the particles were revealed at ~90 emu/g and 70.4 emu/g, respectively. Sodium dodecyl sulfate SDS (95% based on total alkyl sulfate content) was purchased from Sigma Aldrich. In all experiments, deionized water employed was produced by using Purelab Option-Q with resistivity up to 18.2 MΩ·cm from a potable water source. All the chemicals were of analytical grade and used without further purification or treatment.

2.2. Preparation of PVDF Solution

Initially, 10 g of PVDF powder was added into a beaker containing 90 g of DMF solvent with the sensor tip of thermometer immersed into it. After the addition of PVDF powder, this mixture was sealed with parafilm instantaneously while subjecting to constant stirring at 180 rpm. This mixture was then heated from room temperature to 65°C with a heating rate at 10°C/min and was left under this condition with continuous heating for 70 minutes. Immediately after this step, the solution was cooled to 40°C and was left for overnight under constant stirring.

2.3. Preparation of Fe^0/Iron oxides Nanoparticles–PVDF Solution

The NPs-PVDF solution was prepared by the addition of 0.30 g of nanoparticles into 60 g of polymer solution but not vice versa. The mixture had a particle concentration of ~ 0.5wt%. In

order to ensure full dispersion of NPs, direct addition of NP powder into the PVDF solution should be avoided. Here we first dispersed the full amount of NPs into 10 g of PVDF solution contained insides a 20 mL glass valve under intensive sonication for at least 10 minutes. This well-mixed NPs-PVDF solution was then slowly added into the remaining PVDF solution under sonication. All these steps are necessary to ensure the uniform distribution of nanoparticles insides the polymeric solution. The morphology of TODA nanorods and Sigma nanospheres employed in this research was analyzed by Phillips CM12 Transmission Electron Microscope (TEM) with Docu Version 3.2 image analysis software (Fig. 2). The elemental composition of the TODA nanorods and Sigma nanospheres was determined by x-ray diffraction (Bruker Axs D8 Advance) in a range of diffraction angle from 0^{o} to 90^{o} of 2θ.

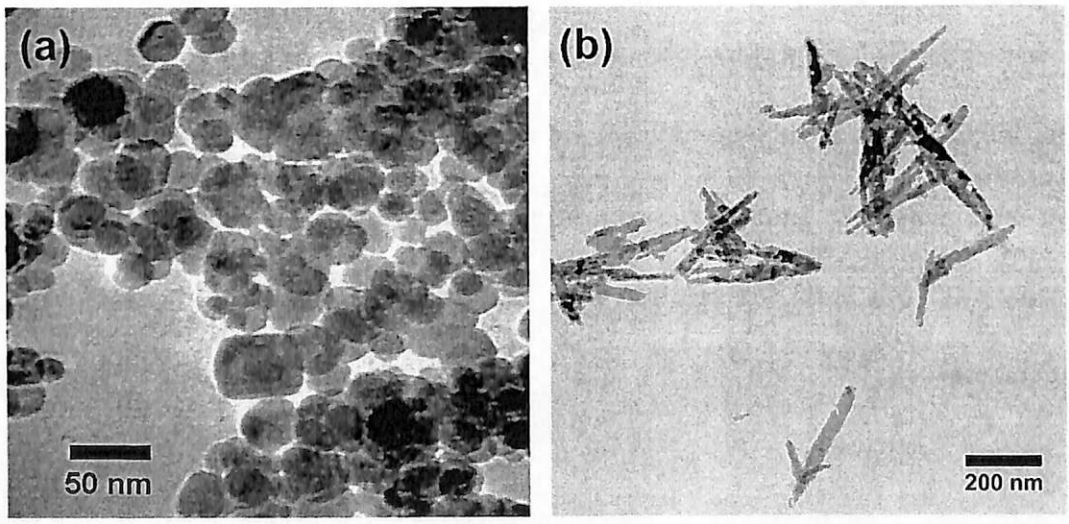

Figure 2. TEM micrographs of NPs employed in this study (a) Sigma nanospheres, and, (b) TODA nanorods.

2.4. Synthesis of Fe^{0}/Iron oxides nanoparticles-PVDF Microcapsules

The experimental setup for the preparation of Fe^{0}/Iron oxides nanoparticles-PVDF

microcapsules is illustrated in Fig. 3. PVDF solution was channeled through a micropipette tip at the pumping speed of around 0.5 mL/min by Watson Marlow Peristaltic Pump followed by drop-wise addition of this polymer solution into a coagulation bath composed of 0.5 wt% Sodium dodecyl sulfate (SDS) in DI water for microcapsules formation. The position of coagulation bath was adjusted manually to avoid the accumulation of microcapsules formed in one single area. Having too many polymeric microcapsules undergoing phase inversion process in one region will promote the fusion of multiple microcapsules together to form doublet, triplet or even a clump of large polymeric clusters. This method was applied to synthesize all three types of microcapsules employed in this study. Fe^0/iron oxides NPs-PVDF solution was sonicated before the synthesis to promote better dispersion of NPs within the polymer solution which subsequently leading to uniform distribution of NPs within the polymeric matrix formed. The internal structure and the overall morphology of microcapsules formed were studied by ZEISS Supra 55 VP Scanning Electron Microscope (SEM) imaging (Fig. 3).

To determine the porosity of the microcapsules formed, we employed the water-to-mass ratio measurement as follow. The weight of water entrapped into the internal pores of microcapsules was determined by heating them mildly inside an oven under 59.7°C-60.3°C and a cabinet under room temperature as controlled sample, respectively. Those microcapsules in oven were weighted for first two hours with five minutes interval between the measurements and were left for overnight; after that, the same samples were weighted again at 30 minutes interval of time for five hours. The same procedure was carried out for samples in cabinet. Both of the samples had been left overnight again after taking the readings for five hours at 30 minutes interval, and the weight data obtained were higher than the former one. This result

showed that microcapsules shrunk after over exposure to the air where no molecular water to support the internal structure of microcapsules; hence, the volume of microcapsules decreased leading to the increase of density. This experiment was carried out at the same time for PVDF, 0.5 wt.% nanorods-PVDF, 0.5 wt.% nanospheres-PVDF microcapsules in order to apply a consistent environmental condition for accurate comparison among them.

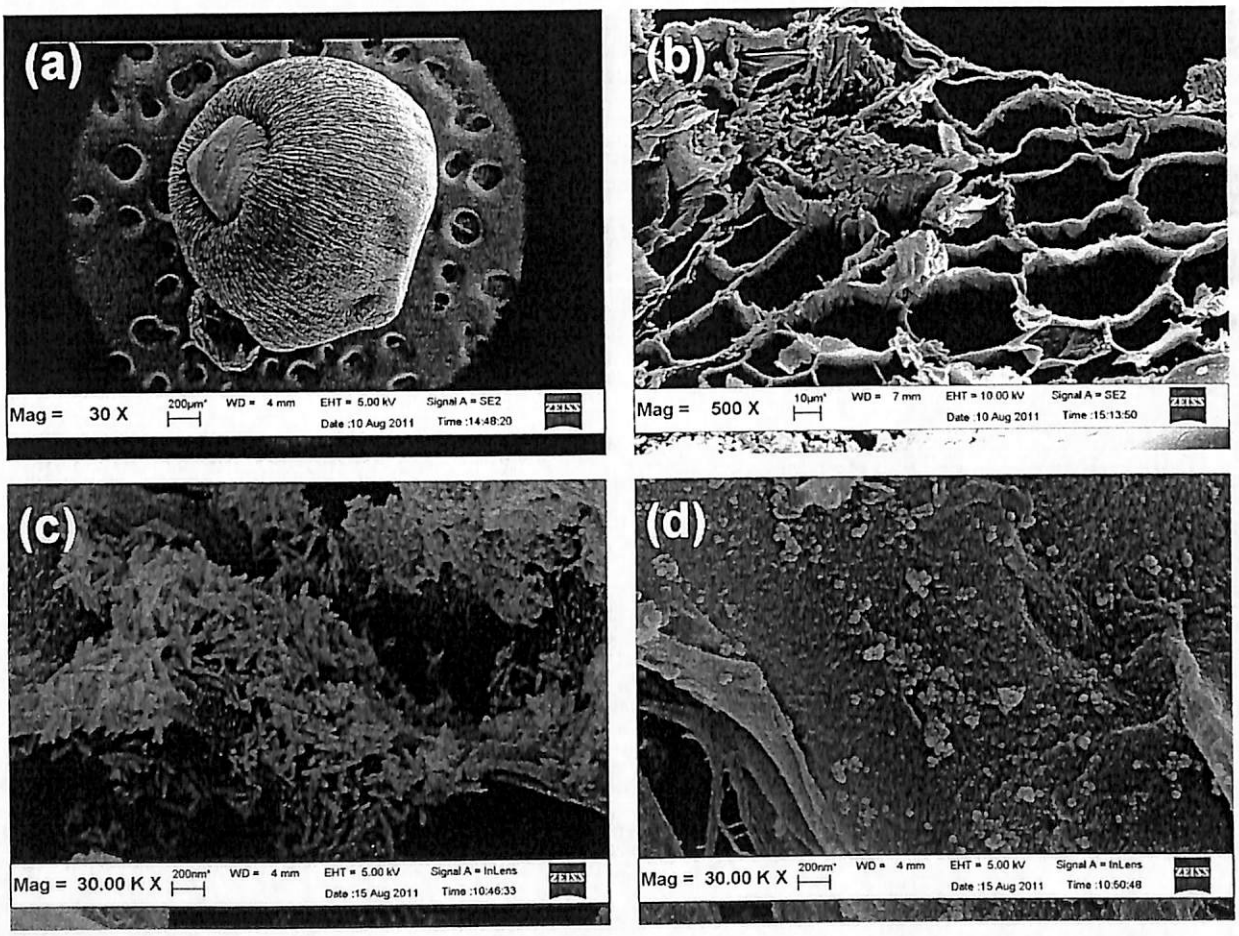

Figure 3. SEM micrographs of synthesized microcapsules (a) entire species of PVDF microcapsule under low magnification showing its outer surface is occupied with small opening, (b) internal porous structure of PVDF microcapsule, (c) internal structure of nanorods-PVDF microcapsule with its inner wall fully covered by nanorod aggregates, and (d) internal structure of nanospheres-PVDF microcapsule with small nanosphere clusters scattered around the inner surfaces.

3. Results and Discussion

3.1. Microcapsule characterization

In this study we chose to construct our 'membrane' according to microcapsule structure as we could take full advantage of the magnetic property of the final structure and also the ease of using it and packing it into modular type. The microcapsule showed a satisfactorily spherical appearance as shown by SEM analysis of Fig. 3, and the averaged diameter of PVDF, nanorods-PVDF, and nanospheres-PVDF microcapsules measured over 100 samples for each sample were 1.845±0.005 mm, 1.845±0.007 mm, and 1.800±0.006 mm, respectively. These values were very close to the size of the PVDF microcapsule sythesized through well-established non-solvent induced phase inversion method at ~ 1.3 mm [15]. The overall structure and size of microcapsule formed is normally depend on the type of solution, amount of SDS surfactant used, diameter of micropipette tip as well as the distance between micropipette tip and surface of coagulation bath. Only under well controlled experiment the spherical structure can be obtained.

As depicted in Fig. 3b-3d, all three species of microcapsules possess very similar porous internal structure, suggesting the formation of three dimensional polymeric network, regardless the presence of NPs. This characteristic porous-structure of microcapsules makes the entrapment of pollutant molecules via diffusion possible with existing concentration gradient across the outer layer of microcapsule as main driving force for this process to happen. After the entrapment of pollutant molecular in the polymeric voids, these molecules adsorbed onto the internal surface of polymer matrix, or/and, undergoing Fenton and Fenton-like reaction catalyzed by Fe^0/iron oxides NPs. However, the aggregation of nanorods (Fig. 3c) onto the

internal surface of PVDF microcapsules, mainly due to the magnetic shape anisotropy effects [19], suggested the need to functionalize the surface of nanorods in order to form a stable NPs dispersion which will lead to more uniform distribution of this particle into the PVDF matrix.

As for the comparison between the nanorod and nanosphere PVDF microcapsules is concerned, nanospheres tend to form smaller clusters scattered all over the internal surface of microcapsules with each cluster composed of limited number of individual nanospheres (Fig. 4d). The extent of agglomeration that leads to the formation of NP clusters, however, is not that severe compared to the case of nanorods. This condition is mainly due to the existence of poly(vinyl pyrrolidone) layer that serves as the steric barrier around the Sigma nanosphere. Nevertheless, this result gives a strong indication suggesting the need for surface functionalization of the NPs prior to their encapsulation into PVDF-network. This step will increase the surface-to-volume ratio of NP, with respect to the microcapsule, that is needed to fully realize its potential for catalytic degradation.

3.2. Test of concept study by using simple organic dye as targeted pollutant

Here Methylene Blue (MB) is chosen as the modelled pollutant at the initial state of our project to test the feasibility of our idea due to its ease of detection by colorimetric method. As clearly depicted in Fig. 4a, the process of MB removal induced by all three types of microcapsules follow a similar trend with rapid initial uptake rate within the range of 0.09-0.22 mg/min and gradually reached a steady state for extended period.

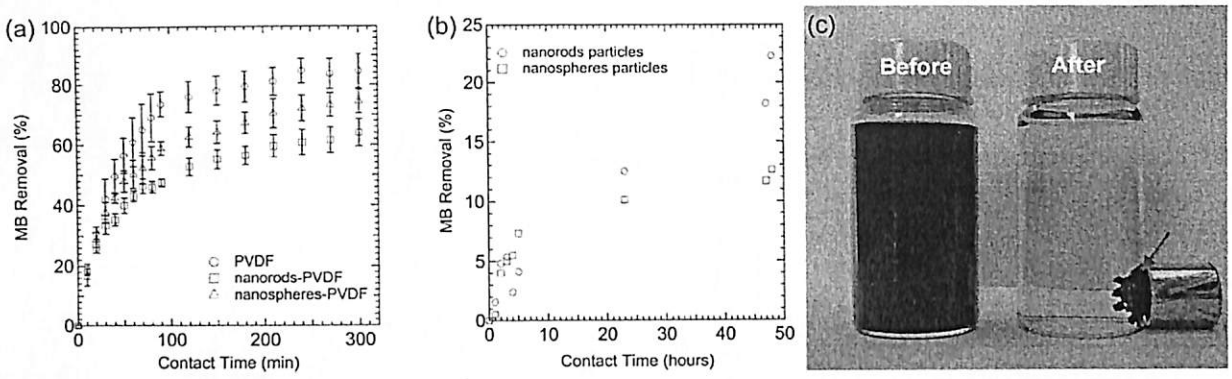

Figure 4. The comparison of MB removal efficiency by using (a) three types of freshly synthesized microcapsules, and (b) the dispersion of nanorods, and nanospheres particles only. For MB degradation processes upto 24 hours by using NPs-microcapsule have resulted total removal percent of 94% for PVDF, 86% for nanospheres-PVDF microcapsules, and 70% for nanorods-PVDF microcapsules. (c) The discolourization of MB caused significant color transition from initial dark blue (100ppm) to light blue. The arrow indicates the collected NPs-PVDF microcapsules.

After the degradation of MB, the NPs augmented microcapsules still retained their magnetic properties and can be easily collected by a NdFeB permanent magnet with a surface magnetic field of ~5500 Gauss (Fig. 5c). The collection was rapid and instantaneous over a distance of few centimeters suggesting the strong magnetic coupling between the magnetic NPs residing within the PVDF microcapsule.

The average void volume of PVDF, nanorods-PVDF and nanospheres-PVDF microcapsules at room temperature is 0.45 cm^3/g, 0.48 cm^3/g, and 0.46 cm^3/g, respectively. In this work, all the PVDF solution prepared was based on the same weight percent of PVDF solution (10 wt% PVDF powder in DMF solvent), and the void volume analysis shows that all three types of microcapsules having very similar internal void space to microcapsules weight irrespective to the presence of NPs. Since the porosity difference among these three microcapsules is

negligible thus it cannot account for the variation witnessed in their capability to remove MB as illustrated in Fig. 5a. Here we hypothesized that there are two main factors contribute to the observation in Fig. 5a in which the fresh PVDF microcapsules out performed NPs-PVDF microcapsules. Firstly, the available surface area of PVDF matrix for MB adsorption plays an important role in this rate determining step. It is clearly shown in the SEM micrographs (Fig. 4c, and 4d) that the nanorods and nanospheres randomly covered up certain portion of the internal surface area of PVDF matrix, hence, slightly reduced the available sites for MB adsorption. If this scenario is true, the total available internal surfaces to accommodate MB should be more in PVDF-only microcapsules compared to both nanospheres-PVDF and nanorods-PVDF microcapsules. This is the main reason for PVDF-only microcapsule out performed both nanospheres-PVDF and nanorods-PVDF microcapsules in MB removal. For freshly synthesized microcapsule, it is very likely that the electrostatic interaction between the MB molecules and the PVDF matrix plays a vital role in MB removal. PVDF is negatively charge due to its largest electronegativity of fluorine [20,21] which favorable attracted positively charged MB molecules [22]. After the adsorption, the Fenton and Fenton-like reactions would be the next immediate step contributes to the MB removal after its partitioning into the PVDF matrix. Fenton and Fenton-like reactions are well known as production methods of free hydroxyl radicals via the presence of Fe together with oxidants (e.g. H_2O_2) [23,24]. The produced free hydroxyl radicals (•OH) degrade the organic pollutants such as dyes by breaking the benzene ring [25,26] and relevant molecules in the structures to simple substances [39]. Hence, the successive adsorbed MB molecules on sorption sites are further degraded.

3.3 Heavy metal and arsenic removal

We further tested the feasibility of using the synthesized microcapsule for heavy metal and arsenic removal. For this purpose we chose cadmium (Cd) as one of the modelled heavy metal pollutant as it has been pervasively found in the waste water from local semiconductor industries. Our results have indicated that Nanosphere-PVDF microcapsule exhibit great advantages compared to nanoparticle alone (and also PVDF microcapsule) in removing a As(III) and As (IV) with removal capacity of 254 µmol/g and also 258 µmol/g. For the case of Cd, we manage to removal almost 99.5 % of Cd in water which translated into a removal capacity of 534.23 µmol/g. This value is almost 20% higher than the typical removal capacity of magnetite nanoparticle reported in literature and we are still working on to understand the mechanism involved [27].

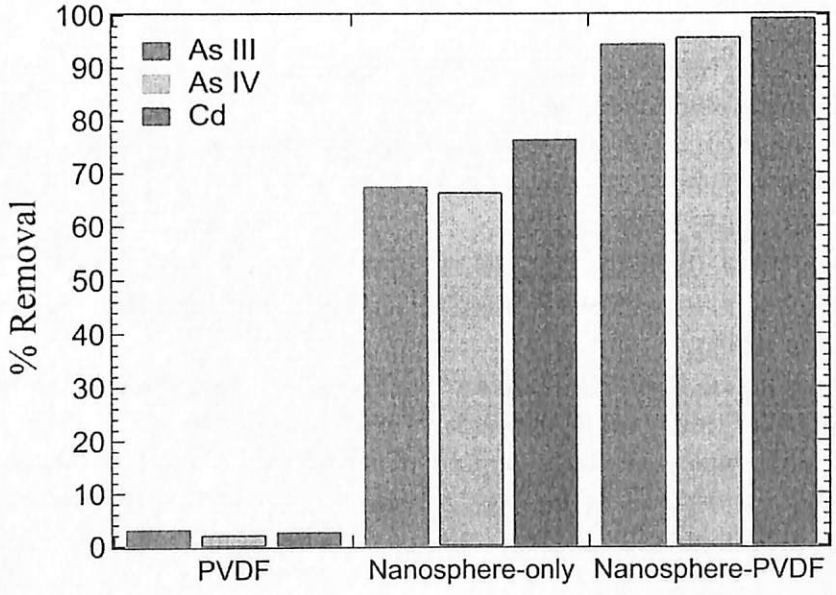

Figure 5. Separation efficiency achieved by using PVDF-microcapsule, nanosphere-only and Nanosphere-PVDF microcapsule in removing As(III), As(IV) and Cd from aqueous environment.

4. Conclusion

We have successfully synthesized magnetic NPs-polymeric microcapsules and demonstrated the engineering applications of this hybrid material on removing methylene blue (MB), As (III), As (IV) and Cd from aqueous environment. The true advantages of using this hybrid materials for environmental applications compared to freely suspended nanoparticles are (i) the risk associated to nanotoxicity has been greatly reduced and (ii) the catalytic and magnetic stability achieved after the encapsulation of Fe^0/iron oxide nanoparticles into polymeric network.

5. References

[1] J. Hu, M.C. Lo, G. Chen, Removal of Cr(VI) by magnetite nanoparticle, Water Sci. Technol. 50 (2004) 139 – 146.

[2] C.T. Yavuz, J.T. Mayo, W.W. Yu, A. Prakash, J.C. Falkner, S. Yean, L. Cong, H.J. Shipley, A. Kan, M. Tomson, D. Natelson, V.L. Colvin, Low-field magnetic separation of monodisperse Fe_3O_4 nanocrystals, Science 314 (2006) 964 – 967.

[3] Y. Liu, S.A. Majetich, R.D. Tilton, D.S. Sholl, G.V. Lowry, TCE dechlorination rates, pathyways, and efficiency of nanoscale iron particles with different properties, Environ. Sci. Technol. 39 (2005) 1338 – 1345.

[4] L.S. Zhong, J.S. Hu, H.P. Liang, A.M. Cao, W.G. Song, L.J. Wan, Self-assembled 3D flowerlike iron oxide nanostructures and their application in water treatment, Adv. Mater. 18 (2006) 2426 – 2431.

[5] J.F. Liu, Z.S. Zhao, G.B. Jiang, Coating Fe_3O_4 nanoparticles with humic acid for high efficient removal of heavy metals in water, Environ. Sci. Technol. 12 (2008) 6949 – 6954.

[6] W. Luo, L. Zhu, N. Wang, H. Tang, M. Cao, Y. She, Efficient removal of organic pollutants with magnetic nanoscaled $BiFeO_3$ as a reusable heterogeneous Fenton-like catalyst, Environ. Sci. Technol. 44 (2010) 1786 – 1791.

[7] J. Feng, X. Hu, P.L. Yue, Degradation of azo-dye orange II by a photoassisted Fenton reaction using a novel composite of iron oxide and silicate nanoparticles as a catalyst, Ind. Eng. Chem. Res. 42 (2003) 2058 – 2066.

[8] B. Saha, S. Das, J. Saikia, G. Das, Preferential and enhanced adsorption of different dyes on iron oxide NPs: a comparative study, J. Phys. Chem. C 115 (2011) 8024 – 8033.

[9] M. Zborowski, L. Sun, L.R. Moore, P.S. Williams, J.J. Chalmers, Continuous cell separation using novel magnetic quadrupole flow sorter, J. Magn. Magn. Mater. 194 (1999) 224 – 230.

[10] J.K. Lim, C. Lanni, E.R. Evarts, F. Lanni, R.D. Tilton, S.A. Majetich, Magnetophoresis of nanoparticles, ACS Nano 5 (2011) 217 - 226.

[11] A. Nel, T. Xia, L. Madler, N. Li, Toxic potential of material at the nanolevel, Science 311 (2009) 622 – 627.

[12] M. Auffan, J. Rose, J.Y. Bottero, G.V. Lowry, J.P. Jolivet, M.R. Wiesner, Towards a definition of inorganic nanoparticles from an environmental, health and safety perspective, Nat. Nanotech. 4 (2009) 634 – 641.

[13] A. Nel, T. Madler, D. Velegol, T. Xia, E. Hoek, P. Somasundaran, F. Klaessig, V. Castranova, M. Thompson, Understanding biophysicochemical interactions at the nano-bio interface, Nat. Mater. 8 (2009) 543 – 557.

[14] M.G. Buonomenna, E. Drioli, Solvent free selective oxidation of benzyl alcohol to benzaldehyde using a membrane contactor unit, Appl. Catal. B: Environ. 79 (2008) 35 – 42.

[15] M.G. Buonomenna, A. Figoli, I. Spezzano, M. Davoli, E. Drioli, New PVDF microcapsules for application in catalysis, Appl. Catal. B 80 (2008), 185 – 194.

[16] M.G. Buonomenna, A. Figoli, I. Spezzano, R. Morelli, E. Drioli, Combined emulsion and phase inversion techniques for the preparation of catalytic PVDF microcapsules, J. Phys. Chem. B 112 (2008) 11264 – 11269.

[17] J.K. Lim, D.X. Tan, F. Lanni, R.D. Tilton, S.A. Majetich, Optical imaging and magnetophoresis of nanorods, J. Magn. Magn. Mater. 321 (2009) 1557 – 1562.

[18] N. Pezeshk, D. Rana, R.M. Narbaitz, T. Matsuura, Novel modified PVDF ultrafiltration flat-sheet membranes, J. Membr. Sci. 389 (2012) 280 – 286.

[19] J. Dubowik, Shape anisotropy of magnetic heterostructures, Phys. Rev. B 54 (1996) 1088 – 1091.

[20] S. Wi, N. Senthilkumar, S-W. Rhee, Characterization of poly(vinylidene fluoride-trifluoroethylene) 50/50 copolymer films as a gate dielectric, J. Mater. Sci: Mater. Electron. 19 (2008) 45 – 50.

[21] X. Li, D. Zhang, S. Chen, H. Zhang, Z. Sun, S. Huang, X. Yin, Dye-sensitized solar cell with higher J_{sc} by using polyvinylidene fluoride membrane counter electrodes, Nano-Micro Lett. 3 (2011) 195 – 199.

[22] S. Kundu, S.K. Ghosh, M. Mandal, T. Pal, A. Pal, Spectrophotometric determination of arsenic via arsine generation and in-situ colour bleaching of methylene blue (MB) in micellar medium, Talanta 58 (2002) 935 – 942.

[23] D. Melgoza, A. Hernandez-Ramirez, J.M. Peralta-Hernandez, Comparative efficiencies of the decolourisation of methylene blue using fenton's and photo-fenton's reactions, Photochem. Photobiol. Sci. 8 (2009) 596 – 599.

[24] K. Dutta, S. Mukhopadhyay, S. Bhatttacharjee, B. Chaudhuri, Chemical oxidation of methylene blue using a fenton-like reaction, J. Hazard. Mater. B84 (2001) 57 – 71.

[25] J. H. Merz, W.A. Waters, The oxidation of aromatic compounds by means of the free hydroxyl radical, J. Chem. Soc. 93 (1949) 2427 – 2433.

[26] P. Sedlak, S. Luhak, J. Brodilova, P. Lederer, Photocatalytic effects of Fe(III) compounds on the hydroxylation of benzoic acid by hydrogen peroxide initiated by uv-radiation, React. Kinet. Catal. Lett. 39 (1989) 249 – 253.

[27] J.F. Liu, Z.S. Zhao, G.B. Jiang, Coating Fe3O4 magnetic nanoparticles with humic acid for high efficient removal of heavy metals in water, Environ. Sci. Technol. 42 (2008) 6949 – 6954.

Highlights:

1. In addition to the main-line of our research, the side-findings from this grant have led to two publications in ISI-cited journals (enclosed as reference):
   (i) Q.H. Ng et al. Sep. Purif. Technol. 132 (2014) 138 – 148.
   (ii) H.X. Che et al. Chem. Eng. J. 243 (2014) 68 – 78.
2. One M.Sc. student, Ms. Kong Li Peng has successfully defended her thesis on Nov 2013 based upon the works presented in this report.
3. The high speed centrifuge bought under this grant is very useful and has benefited the research program of JK Lim (PI of this grant) in long run.

Appendix

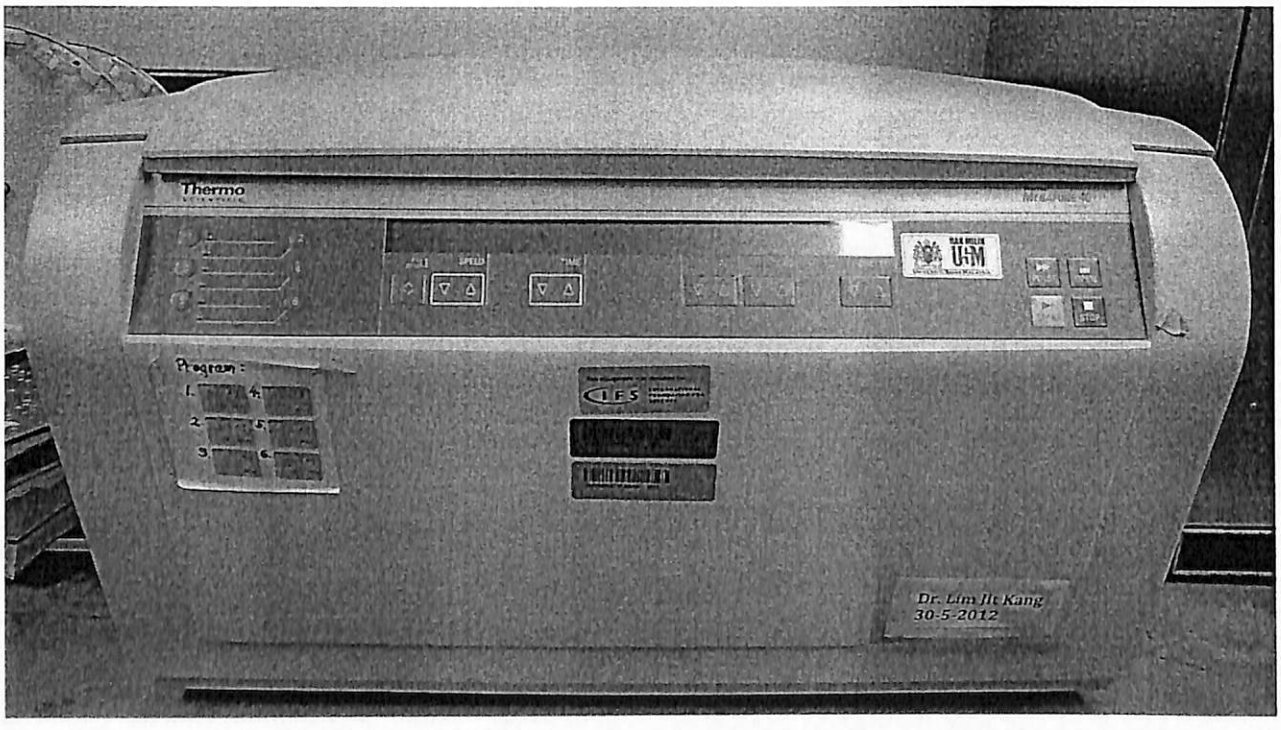

Thermo Scientific Ventilated Centrifuge model Megafuge 40 – 3 L bought under this grant. This equipment is currently located in Research Lab of JK Lim in School of Chemical Engineering, Universiti Sains Malaysia.

IFS

Report Of Project Expenditures Using Transferred Funds(*)

Instructions: This form is to be completed following the completion of an IFS supported research project. In the spaces provided below please provide information pertaining to any IFS funds that were transferred to your institution for the purchase of research supplies and services. This form should be returned to IFS together with your application for a renewal grant and/or your final report to IFS.

IFS Grant Agreement No. W/5098-1

Amount of grant approved by IFS: **MYR 33,078** **(USD 11,200)**

Amount transferred to your institution: **MYR 33,078** **(USD 11,200)**

Transferred funds were spent on**:	Amount in MYR:	Supplier (company name and country)
Equipment Thermo scientific ventilated centrifuge model Megafuge 40 – 3 L (see appendix for photo)	RM 12, 500	Thermo Fisher, Malaysia
Service ICP OES Analysis		NM Laboratory Sdn Bhd, Malaysia
Vibrating Sample Magnetometry (VSM) measurement	RM 4,921.70	Arkival Technology Corporation, USA
X-Ray Diffraction/ICP MS		Universiti Sains Malaysia, Malaysia
Supplies Lab supplies and chemicals	RM 14,551.45	PLC Solution, Malaysia Fisher Scientific, Malaysia Modern-Lab Chemicals, Malaysia China Rare Earth Magnet Limited, China DKSH Technology, Malaysia Arachem (M) Sdn Bhd, Malaysia SHXP Trading, Malaysia Chemglass Life Science, USA
Other (please specify): Internal purchase	RM 826.95	Universiti Sains Malaysia, Malaysia
Left Over Budget	RM 277.90	Universiti Sains Malaysia, Malaysia

(*) Please feel free to write about your experiences with regard to the transfer of the grant and purchasing matters on the reverse side of this paper or on a separate page.

(**) List equipment items, categories of expendable supplies (eg glassware, reagents, etc), literature (eg books, journals, reprints, etc), local travels (no of trips, destination), extra manpower (no of persons, duration of employment), other expenditures (must be specified).

Date and Signature of the Principal Investigator

Oct 03, 2014

Dr. Lim Jit Kang
Senior Lecturer
School of Chemical Engineering
Universiti Sains Malaysia

Date and Signature

For the Institution

MOKHTAR ALFAKARI ANSORI
Ketua Penolong Pendaftar
Pusat Pengajian Kejuruteraan Kimia
Kampus Kejuruteraan
Universiti Sains Malaysia

7/10/14

Name and Position (type)

PROFESOR AZLINA HARUN @ KAMARUDDIN
Dekan
Pusat Pengajian Kejuruteraan Kimia
Kampus Kejuruteraan
Universiti Sains Malaysia, Seri Ampangan
14300 Nibong Tebal, Seberang Perai Selatan
Pulau Pinang.

Separation and Purification Technology 132 (2014) 138–148

Contents lists available at ScienceDirect

Separation and Purification Technology

journal homepage: www.elsevier.com/locate/seppur

Efficacy evaluation of the antifouling magnetite–PES composite membrane through QCM-D and magnetophoretic filtration performances

Q.H. Ng [a], J.K. Lim [a,b], A.L. Ahmad [a], B.S. Ooi [a], S.C. Low [a,*]

[a] School of Chemical Engineering Campus, Universiti Sains Malaysia, Seri Ampangan, 14300 Nibong Tebal, S.P.S. Penang, Malaysia
[b] Department of Physics, Carnegie Mellon University, Pittsburgh, PA 15213, United States

ARTICLE INFO

Article history:
Received 22 November 2013
Received in revised form 5 May 2014
Accepted 6 May 2014
Available online 23 May 2014

Keywords:
QCM-D
Membrane fouling
Magnetophoretic actuation
Water treatment

ABSTRACT

This study presents the surface interactions and macromolecular properties of magnetic responsive polyethersulfone (PES) membranes in relation to their potent antifouling behavior. Polyelectrolytes, polyanion poly(sodium-4-styrene-sulfonate) (PSS) and/or polycation poly(diallyldimethylammonium chloride) (PDDA), were alternately adsorbed on the surface of a PES microfiltration membrane using the polyelectrolyte multilayer modification method. Subsequently, the magnetic responsive Fe_3O_4 functional layer was end-capped to the polyelectrolytes-assembled-PES membrane. By using a quartz crystal microbalance with dissipation (QCM-D), the viscoelastic properties (ΔD) and adsorption kinetics (Δf) of the adsorbed adlayers were investigated. The QCM-D results demonstrated an exponential growth of Fe_3O_4 nanoparticles on the polyelectrolytes-assembled-PES polymer. The changes in the dissipation factor (ΔD) show greater motional freedom of the deposited multilayers (PSS, PDDA and Fe_3O_4) on the surface of the PES, where the surface morphology for the PES–Fe_3O_4 membrane was elucidated using FESEM/EDS. In this study, the synthesized magnetic responsive PES–Fe_3O_4 membrane demonstrated significantly improved permeability and selectivity. The membrane was shown to have a higher resistance to fouling based on the actuation motions of the magnetic nano-colloid under an oscillating external magnetic field. Subsequent exposure to a twisting effect promoted the detachment of humic acid from the membrane.

1. Introduction

Membranes used for potable water production have remarkably progressed over the past few years due to compact design of the membrane module, lowered energy consumption, and reliable effluent quality [1,2]. Nevertheless, membrane fouling caused by the deposition of fouling materials on the membrane remains a critical issue in all applications of water filtration processes and is the dominant factor that restricts the widespread application of membranes. Membrane fouling generally reduces performance by declining filtrate flux, resulting in increases of the operating and replacement costs. Hence, several approaches to mitigating membrane fouling have focused on changing the feed stream conditions (e.g., pH, ionic strength, flocculation and coagulation processes) [3,4], developing chemical cleaning technologies [5] and modifying the membrane surface to alter the surface charge, roughness and membrane hydrophilicity [2,6,7].

Under water treatment, humic acid (HA), which is an important precursor to trihalomethane and haloacetic acids, has been considered one of the most significant foulants among many potential natural organic matter (NOM) in both surface and ground water [8,9]. A number of studies about membrane fouling have focused on the role of several important properties of HA solutions [8,10–12]. For example, membrane fouling increases with decreasing pH or increasing ionic strength (e.g., increasing the electrolyte concentration or adding of divalent cations) of HA solutions [8,10,12]. The existence of the divalent cations in the feed stream, such as Ca^{2+}, increases membrane fouling due to the formation of the HA divalent cation complex, as observed in many studies using various types of membranes [8,12]. However, these types of research approaches are labor intensive and normally require tedious analysis of the feed stream before filtration processes.

In general, hydrophilic membranes exhibit lower levels of fouling and increased flux reversibility at their surfaces [2]. Thus,

* Corresponding author. Tel.: +60 4 5996412; fax: +60 4 5941013.
E-mail addresses: chsclow@usm.my, siewchun@gmail.com (S.C. Low).

http://dx.doi.org/10.1016/j.seppur.2014.05.019
1383-5866/

many approaches have improved the hydrophilicity of membranes, including blending hydrophilic polymers in the casting dope and modifying the membrane surface through polymerization, polyelectrolyte adsorption, plasma modification or chemical modification such as sulfonation [6,13–17]. However, the polymer chain undergoing chemical modification sometimes becomes highly swollen, leading to a decrease in the effectiveness of the membrane's mechanical properties [18].

The use of nanoparticles in the manufacturing of membranes allows the formation of inorganic polymer composites with specific functionalities, contributing to better membrane performances with increasing permeability, selectivity, and a higher resistance to fouling. In particular, the beneficial effects of nanoparticle-based membranes on the mitigation of membrane fouling have been reported from many research groups [7,19–22]. The integration of nanoparticles into the polymeric matrix can be achieved by various techniques, such as polyelectrolyte multilayer modification (PEM), self-assembly through covalent attachment or blending within the casting dope [7,23–25]. A few studies that utilized the magnetic properties of Fe_3O_4 in synthesizing the magnetite composite membranes have successfully demonstrated the separation of specific substances by altering the magnetic intensity [26,27]. In our study, we have targeted of different approaches in which we deposited Fe_3O_4 onto the membrane surface. The actuation motion of the magnetic nano-colloids was created at the membrane surface by the oscillating external magnetic field sources, which in turn promoted the detachment of the foulants from the membrane surface.

Quartz crystal microbalance with dissipation (QCM-D) monitoring measurement is a surface sensitive technique that provides real time information by measuring the changes in mass and viscoelastic/structural properties at the deposited layer surface. This technique has been used to characterize the surface adsorption kinetics of thin film layers and offers the opportunity to analyze the surface interactions of the nanoparticle–polymer in real time [28,29]. Few reports have presented the effectiveness of the QCM-D technique in evaluating the adsorption and viscoelastic properties of foulants (organic and inorganic) on different types of membrane surfaces [30–32]. For example, Hashino and co-workers [32] utilized the QCM-D technique to analyze the adsorption of foulants, such as sodium alginate (SA), bovine serum albumin (BSA) and humic acid (HA), on a cellulose acetate butyrate (CAB) membrane. Based on the QCM-D measurement, the mass adsorbed on the quartz crystal calculated using the Sauerbrey equation showed that the adsorbed BSA (approximately 3.3 mg/m^2) was much greater than those of SA and HA (approximately 0.2 mg/m^2) [32]. In our studies, QCM-D technology was used to investigate the interaction affinity between functionalized magnetite nanoparticles (F-MNPs) or modeled foulant (e.g., HA) with a specific surface. The QCM-D is used to rule out the deposition contributions of F-MNPs on different modified polyethersulfone (PES) membrane surfaces. Besides, it has also been utilized to study the adsorption and detachment of HA from the membrane surfaces, in order to investigate the antifouling mechanism in presence of F-MNPs.

In this study, we aimed to quantify the adsorption of PSS-coated Fe_3O_4 nanoparticles (F-MNPs) on the surface of PES membranes using QCM-D measurements in the presence of precursors comprising different combinations of polyelectrolytes (e.g., polyanion PSS and polycation PDDA). Moreover, before end-capping the F-MNPs to the surface of the PES membrane, the F-MNP colloids were dispersed in two different types of dispersants, i.e., deionized (DI) water or PSS solution. The effect of dispersant type on the deposition of F-MNPs on the surface of the PES membrane was also elucidated. To prove the functionality of this magnetic responsive nano-composite membrane, filtration studies were carried out at conditions with or without an external magnetic field. Both the permeation and rejection performances for the HA foulant were discussed.

2. Materials and methods

2.1. Materials

The magnetite nano-colloid iron oxide Fe_3O_4 was supplied by NanoAmor (Houston, Texas, USA). PSS (average MW approximately 70,000 Da) and PDDA (MW 100,000–200,000 Da, 20% aqueous solution) were purchased from Sigma–Aldrich (St. Louis, MO, USA). Flat sheets of PES microfiltration membranes with a 0.1 μm pore size were obtained from Koch (Wilmington, Massachusetts, USA). PES polymer (Ultrason E6020P with MW 58,000 Da) was supplied by BASF (Ludwigshafen, Germany) and was used as the model polymeric membrane material which coated on the quartz crystal cell for QCM-D analysis. The solvent N-methyl-2-pyrrolidone (NMP) was purchased from Merck (Darmstadt, Hessen, Germany). Humic acid purchased from Sigma–Aldrich (St. Louis, MO, USA) was used as the organic foulant. 1 M of NaOH (Merck, Darmstadt, Hessen, Germany) and 1 M of HCl (analytical reagent grade, 37%; obtained from Fisher Scientific) were used for pH adjustment. All the chemicals were used as received without further purification or modification.

2.2. Functionalization of nanoparticles

PSS dissolved in DI water (0.02 mol L^{-1}) was prepared and ultrasonicated to promote good dispersity and dissolution of the PSS polymeric solution. Similarly, a suspension with 2500 mg L^{-1} of Fe_3O_4 was prepared in DI water and ultrasonicated to break the existing aggregates. pH of Fe_3O_4 suspension and PSS solution were adjusted to 3.5 before the former was added drop-wise into the latter solution. The physisorption of PSS on Fe_3O_4 via electrostatic attraction was allowed to occur for 1 day on an end-to-end rotating mixer with a mixing rate of 40 rpm. The F-MNPs were then separated from the PSS solution with a permanent magnet and pre-washed to remove excess PSS from the F-MNPs before the final dispersion in DI water or PSS solution. The bare nanoparticles (Fe_3O_4) started to flocculate from their initial hydrodynamic diameter of approximately 306 nm to form the larger clusters up to approximately 2000 nm (data not shown). However, after the bare Fe_3O_4 particles were functionalized with PSS, the cluster size dramatically reduced to approximately 145 nm.

Dynamic light scattering (Zetasizer Nano ZS900-Malvern Instruments Ltd., UK) was used to determine the hydrodynamic size and zeta potential of F-MNPs and polyelectrolytes (PSS and PDDA, pH 3.5). A light scattering from a laser beam of $\lambda = 633$ nm was operated at backscattering mode at angle 173°. The hydrodynamic diameters of Fe_3O_4 and its size distribution profile in function of time were monitored by dispersing 7.2 μL of the magnetite suspension (2500 ppm) into 3 mL of DI water. All of the samples were measured in triplicate to confirm the reproducibility of the results.

2.3. Quartz crystal microbalance with dissipation (QCM-D)

The QCM-D measurements were performed using the AT-cut quartz crystals mounted in an E1 system (Q-sense, Goteborg, Sweden). Quartz crystals coated with gold were obtained from Q-sense, Sweden. A comparable PES membrane surface (1% (w/v) PES solution in NMP) was spin coated on the surface of the quartz crystal cell to study the dynamic adsorption of F-MNPs, the precursors (PDDA and PSS) and HA onto the PES membrane surface. The

PES coated quartz crystal cell was then inserted into the QCM-D chamber, where the polymer coated side was faced to the flow-through liquid. All QCM-D measurements were conducted under flow-through conditions via a digital peristaltic pump (Ismatec, IDEX) operating in sucking mode at a constant flow rate of 50 μL min^{-1} and a temperature of 25 °C. Frequency and dissipation shift as a function of time induced by the addition of PSS/PDDA/F-MNPs/HA solutions were recorded.

2.3.1. Adsorption kinetics of F-MNPs

The dynamic adsorption of F-MNPs (either dispersed in DI water or PSS solution) and of the polyelectrolytes precursors (polyanion PSS and/or polycation PDDA) on the PES surface was monitored using QCM-D. The different combinations of the magnetic responsive PES membrane are shown in Fig. 1. All masses adsorbed of the multilayers for each combination (Fig. 1) were modeled based on viscoelastic model in QTools provided by Q-sense.

2.3.2. Monitoring of HA adsorption and cleaning from the membrane surfaces

The adsorption and desorption (cleaning process) of HA foulant from the surfaces of the magnetic responsive PES–Fe_3O_4 membranes and the unmodified neat PES membranes were investigated using QCM-D. The HA foulants (25 ppm) were first allowed to flow across the modeled PES membrane surface via digital peristaltic pump operating in suction mode at a constant flow rate of 50 μL min^{-1} at temperature of 25 °C for 2 h. Subsequently, cleaning process (desorption of HA from the quartz crystal cell) was carried out by flow through the DI water, utilizing the same pump suction flow rate of 50 μL min^{-1} for 30 min. Both the adsorbed and desorbed masses of HA from the quartz crystal surface were calculated using QTools software, as described by the Sauerbrey equation [33]:

$$\Delta f = -\frac{n}{C}\Delta m \quad (1)$$

where Δf refers to the changes of frequency (Hz), Δm refers to the changes of mass adsorbed (HA) per surface area of the quartz crystal cell (ng cm^{-2}), n is the overtone number (n = 3 in this study) and C is the mass sensitivity constant of the QCM-D (C = 17.7 ng cm^{-2} Hz^{-1} at f = 4.95 MHz).

2.4. Development of magnetic responsive PES membrane

A flat microfiltration PES membrane that served as the support layer was placed on a glass plate fitted onto the vacuum chuck of the spin coater (Interscience G3P-8, USA). Subsequently, the polyelectrolyte solutions (PSS and PDDA) at 0.02 mol L^{-1} were alternately deposited onto the PES membrane. The negatively charged PSS solution served as the first deposition layer on the PES membrane surface through the hydrogen bonding and hydrophobic interaction [7], followed by the positively charged PDDA solution. The third and top functional layer was the magnetic responsive F-MNPs. All deposited layers were spin coated at a spinning rate of 3000 rpm with a rotation time of 8 s. The fluid was spun off the edges of the substrate until a desired homogeneous thin film magnetophoretic polymer was formed.

The top surface morphology and cross section of the neat PES and modified magnetic responsive PES membranes was analyzed under field emission scanning electron microscope (FESEM, Quanta FEG 450, and Netherlands). Using the same sample in FESEM, the quality of the dispersion and existence of Fe_3O_4 particles on the membrane surface and top layer on cross section of membrane were analyzed using energy dispersive spectroscopy (EDS, Quanta FEG 450, and Netherlands).

2.5. Membrane filtration and rejection performances

Approximately 0.1 g of humic acid powder was dissolved in 2 L of DI water to serve as the organic foulant in the aqueous feed. Prior to the filtration study, HA feed solution (50 ppm) was adjusted to pH 8.0 by using 1 M of NaOH or HCl solution. For the filtration study, the membrane was placed in a 25 mm diameter dead-end stirred cell (Model 8010, Millipore Corp., Bedford, MA) with an effective membrane area of 4.1 cm^2 connected to an ultra-pure grade nitrogen-pressurized 1 L solution reservoir. The reservoir and stirred cell were initially filled with DI water. The pure water fluxes (J_0) for all neat and modified membrane were measured at the constant low pressure of 10 psi, where a quasi-steady flux was achieved (usually within 30 min). Only those membranes with deviation in J_0 less than 10% from the median value (neat PES membrane J_0 = 27 L m^{-2} h^{-1} and composite magnetite membrane J_0 = 21 L m^{-2} h^{-1}) were used for further experiments. The reservoir and stirred cell were then replaced by the HA solution to carry out the fouling study. To study membrane fouling, the filtration was carried out for 12 h at an applied pressure of 10 psi. The accumulated permeate mass which will be used to calculate the filtration flux (J) was read by a computer-recorded electronic balance (FX3000i AND, USA) at an interval time of 20 s. The concentrations of HA obtained from the accumulated permeate were then measured using a UV–Vis spectrophotometer (Pharo 300 Spectroquant, Merck Millipore) at the wavelength of 254 nm.

To investigate the effectiveness of the magnetic responsive PES membrane for potent antifouling behavior, an in-house fabricated magnetic field rotator connected to a magnetic source and a PLC controlled rotator was used, as shown in Fig. 2. During the filtration processes, the PLC controlled rotator was set to change the position of the magnet field source every 20 s. The introduction of the magneto-induced rotation motions aligned the F-MNPs in

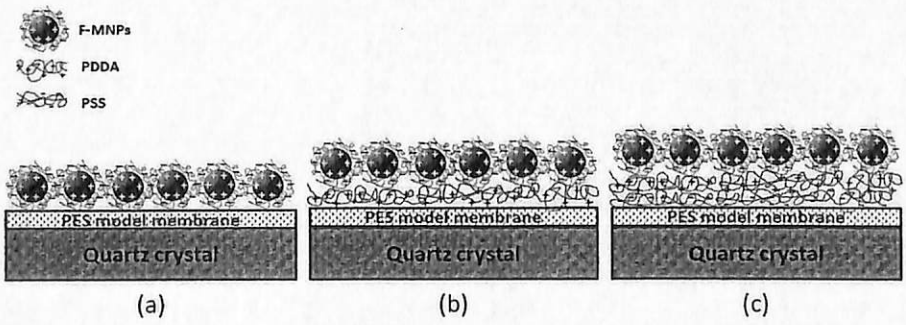

Fig. 1. Schematic of the different combinations. Deposition of F-MNPs (a) without precursor, (b) coated with the precursor of polycation PDDA, and (c) coated with the precursors of polyanion PSS and polycation PDDA.

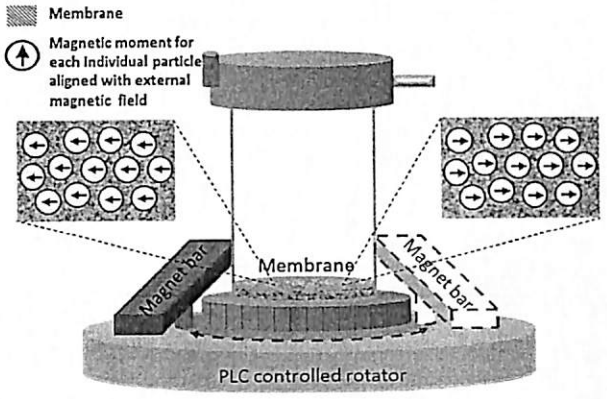

Fig. 2. Schematic diagram for the dead-end filtration cell, showing the positioning of the magnetic field source controlled by a PLC rotator. The magnetic bar setup can be arranged by either pointing the north poles to or away from each other.

a single direction at the specific interchange position. Subsequently, promoting the magnetophoretic actuation of F-MNP colloids on the membrane surface further detached the foulants from the membrane surface.

3. Results and discussion

3.1. Quantitative measurement of the adsorbed F-MNP composite film on different PES modified membranes

Prior to the end-capping of F-MNPs to the PES membranes, the F-MNP colloids were first dispersed in either DI water or PSS solution to ensure the mono-dispersity of the F-MNP composite film on the membrane surfaces. As per an earlier hypothesis, the presence of free polyelectrolyte (PSS) molecules in the F-MNP suspension is expected to assist in the higher adsorption of the F-MNP colloids onto the surface of the PES membrane, due to the electrostatic interactions. However, the experimental outcomes exemplified another way. For all assembled multilayer conditions (illustrated in Fig. 3a–c), change in both frequency and dissipation were observed for the lower mass deposition of the F-MNP composite layer when the F-MNP colloids were dispersed in the PSS solution (conditions 1a–c) compared with the F-MNP colloids dispersed in DI water (conditions 2a–c).

The larger Δf_3 frequency shift in Fig. 3a–c at condition 2 (dispersed in DI water) indicated a greater mass adsorbed of F-MNPs on the membrane surface. The large mass of deposited monodispersed F-MNP colloids might respond better to the magneto-induced actuation motions. When the F-MNP colloids were dispersed in PSS solution, a lower frequency shift or mass deposition of F-MNPs was observed, indicating a poor deposition of the F-MNP thin film composite on the membrane surface (for all multilayer conditions in Fig. 3a–c). This result is likely because an adsorption competition existed between the F-MNP colloids and the free PSS polyelectrolytes at the top surface layer of the PES coated quartz crystal. As shown in Table 1, both the F-MNPs and the free PSS polyelectrolytes were negatively charged. In fact, the free PSS polyelectrolyte has the highest negative charge density at -63.4 ± 3.41 mV compared with the F-MNP colloids at -40.53 ± 0.81 mV. Hence, it is possible to induce a higher adsorption affinity to the surface of the PES-coated quartz cell for the free PSS polyelectrolytes. In contrast, fewer adsorption sites were available for the F-MNP colloids to attach to, which contributed to the lower deposition mass.

To explain the competitive adsorption phenomenon existing between the F-MNP colloids and the free PSS polyelectrolytes, additional adsorption kinetic analyses for the free PSS polyelectrolytes were carried out. For the analyses, the PES-coated quartz cell is first coated with a layer of polyanion PSS, followed by the subsequent adsorption of a layer of polycation PDDA. The ΔD versus Δf plots (Fig. 4) show differences between not only the amounts of adsorption for both F-MNPs dispersed agents (DI water and PSS solution) but also the viscoelastic characteristics of the film adsorbed. The adsorption kinetic analysis clearly noted limited adsorption capabilities for the F-MNP colloids dispersed in PSS (Fig. 4b). The frequency shift of F-MNP colloids dispersed in PSS was smaller (approximately 15 Hz, Fig. 4b3) compared with that of the F-MNP colloids dispersed in DI water (approximately 350 Hz, Fig. 4a3) at the 3rd layer Δf_3 F-MNP adsorption step. Interestingly, the trend of the ΔD_3 versus Δf_3 profiles for the pure PSS solution without the presence of F-MNPs (Fig. 4b, gray line) was shown to be similar to that of the F-MNPs dispersed in the PSS solution (Fig. 4b, black line), demonstrating a similar adsorption and desorption mechanism was took place. This observation shows that only PSS polymer was adsorbed to the membrane surface instead of the F-MNP colloids. Based on the analysis up to this point, DI water was selected as the dispersant to disperse the F-MNP colloids before end-capping to the modified PES membrane.

As for the interaction effects of the PSS and PDDA precursors to the adsorption of F-MNPs, three different precursor layers were examined, as referenced earlier in Figs. 1 and 3 of the QCM-D adsorption frequencies (conditions a–c). The quantitative masses adsorbed of the F-MNPs on each of these conditions were calculated based on the viscoelastic model, as presented in Fig. 5. Each small plateau in the figure represents the particular adsorption layer (PSS then PDDA then F-MNPs) that obtained continuously throughout the QCM-D analysis. The results showed that when neither polyanion PSS nor polycation PDDA was deposited, the lowest mass of F-MNPs (approximately 18 mg/m^2) was adsorbed on the PES surface (Fig. 5a). In the absence of strong polyelectrolytes, the interaction between the F-MNP colloids and the PES membrane was weakly retained via weak hydrogen bonding and hydrogen–hydrogen interactions [7]. Consequently, less adsorbed F-MNP colloids was observed.

The presence of polyelectrolyte precursors (Fig. 5b and c) on the PES membrane before the final end-capping of the F-MNPs contributed to the greater mass adsorption of F-MNPs to the quartz cell. In comparing a single coated layer of polycation PDDA (Fig. 5b) with a bilayer coating of polyanion PSS and polycation PDDA (Fig. 5c), the latter bilayer combination contributed to a greater mass adsorbed of F-MNPs (approximately 126 mg/m^2) compared with the former single coated PDDA layer (approximately 77 mg/m^2). In the latter bilayer combination, the PSS precursor first interacted with the PES surface via hydrophobic interactions [34] followed by the assembly of polycation precursor PDDA through strong electrostatic interactions. The multilayer (PES → PSS → PDDA) formed a strong "polycation blanket" with a strong positively charged outermost layer on top of the membrane surface [35]. Thus, the negatively charged F-MNP colloids were able to firmly deposit on the top surface of the model membrane (approximately 126 mg/m^2).

As compared with only a single layer of weakly adsorbed PDDA on a PES surface (PES → PDDA), the interaction between the precursor PDDA and PES was maintained through hydrophobic interactions. Thus, a physically lower binding strength to the membrane decreased the number of positive binding sites available on the membrane surface. Consequently, this resulted in a reduced attraction for negatively charged PSS-functionalized MNPs and resulted in fewer attachments of F-MNP colloids to the membrane (approximately 77 mg/m^2). These results have shown that the use of polyelectrolyte multilayer modification (PEM) increases the adsorption of F-MNPs to the surface of the PES membrane. It is expected that additional polyelectrolyte layers would produce a continuous film

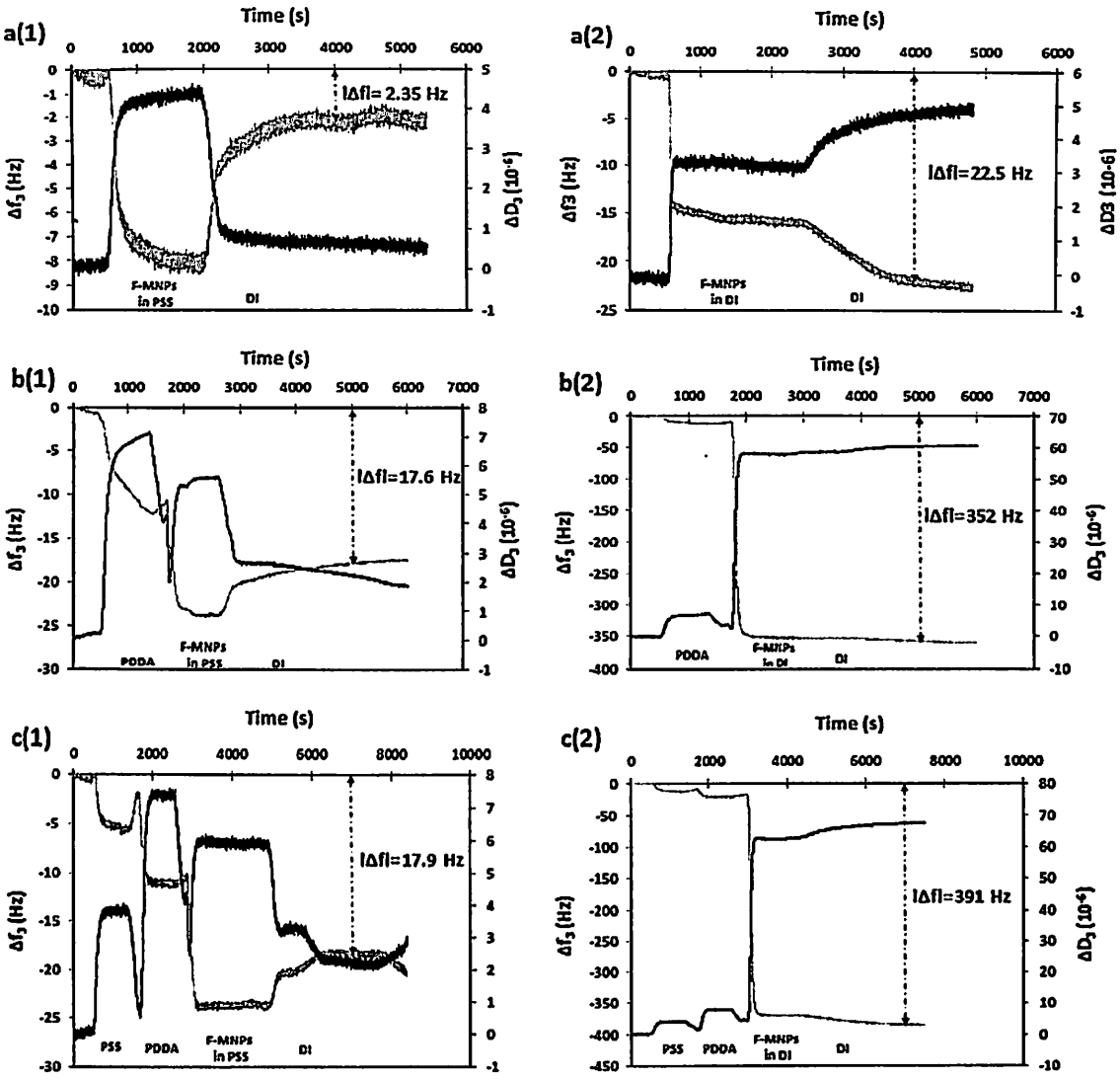

Fig. 3. The frequency (gray line) and dissipation (black line) changes for the 3rd overtone as a function of time during adsorption of composite film F-MNPs dispersed in (1) PSS solution and (2) DI water on different PES-coated crystal cells: (a) PES-coated quartz cell without polyelectrolyte precursor, (b) PES-coated quartz cell coated with polycation PDDA precursor, and (c) PES-coated quartz cell coated with polyanion PSS and then polycation PDDA precursors. The overall deposition mass was represented by the frequency changes ($|\Delta f|$).

Table 1
Zeta potential measurement for the polyanion (PSS) and polycation (PDDA) polyelectrolytes and the magnetite nanoparticles (F-MNPs).

Polyelectrolyte	Zeta potential (mV)	
	Average	Standard deviation
PSS	−63.40	3.41
PDDA	+63.83	3.76
F-MNPs	−40.53	0.81

with an increased surface charge (positively charged in this study) and additional ion-exchange sites for the adsorption of F-MNPs [15,34,36]. However, only a single bilayer of PSS/PDDA was applied in current study in order to reduce the overall membrane thickness and compactness for minimum membrane transport resistance.

A rinsing step with DI water was performed to confirm the binding strength of F-MNPs to the membrane surface. During the rinsing step, DI water was perfused across the F-MNP-capped PES membrane for 1 h, as illustrated in Fig. 5a–c. The results showed almost no detachment of F-MNPs from all coated surfaces and a slight increase of the overall mass. This mass increase was most likely due to swelling within the PEM layer (alternate adsorption of PSS and PDDA) on the porous support PES matrix [37,38]. The formation of the layer through ionic crosslinking between polyions may increase the porosity of the film enabling an increased adsorptive capacity for free water molecules [39]. The amount of swelling was dependent on the degree of ionic crosslinking within the layer [34] and also on the ion charge at the layer end [37].

3.2. Antifouling behavior of magnetic responsive PES membranes

Based on the QCM-D measurements, two precursor layers (PSS + PDDA) which help in increasing the final deposition of magnetite nanoparticles gave the highest deposition of F-MNPs (126 mg/m^2 in Fig. 5c) on the membrane surface. The high deposition of F-MNPs is expected to provide better actuation motions of F-MNPs, which promote the detachment of foulant from the membrane surface. Thus, membrane filtration performance tests were carried out to investigate the antifouling capability of the magnetic

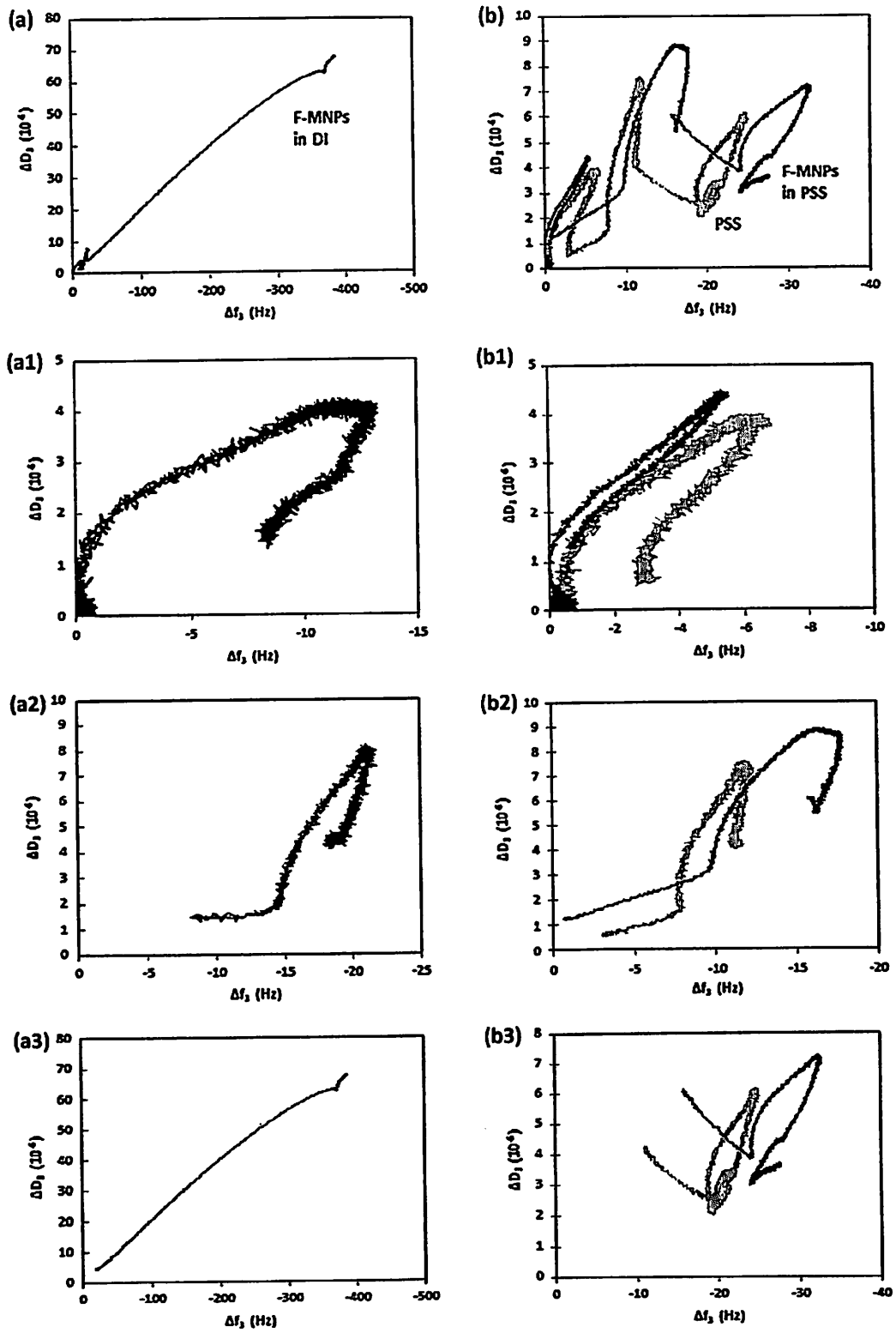

Fig. 4. The 3rd overtone dissipation change (ΔD_3) versus frequency shift (Δf_3) profile for the adsorption of (a) F-MNPs dispersed in DI water, (b) F-MNPs dispersed in PSS solution (black line) and blank PSS solution without F-MNPs (gray line) on the surface of the modified PES quartz cell. (a1 and b1) Refer to the first coated layer of PSS followed by a DI water rinsing step. (a2 and b2) Refer to the second coated layer of PDDA followed by a DI water rinsing step. (a3) Refer to the third/top functional layer of the magnetic responsive F-MNPs in DI water followed by a DI water rinsing step, (b3) refer to the F-MNPs dispersed in PSS solution (gray line) and the blank PSS solution without F-MNPs (black line) followed by a DI water rinsing step.

responsive PES membrane (composite layer consisted of PSS, PDDA and F-MNPs), in removal of humic acid foulants. Firstly, two precursor layers (PSS + PDDA) followed by F-MNPs were spin-coated on the membrane surface. FESEM micrographs (Fig. 6) clearly show the dispersion of the F-MNP colloids on the membrane surface. As shown in the FESEM micrographs, the smooth surface of the neat

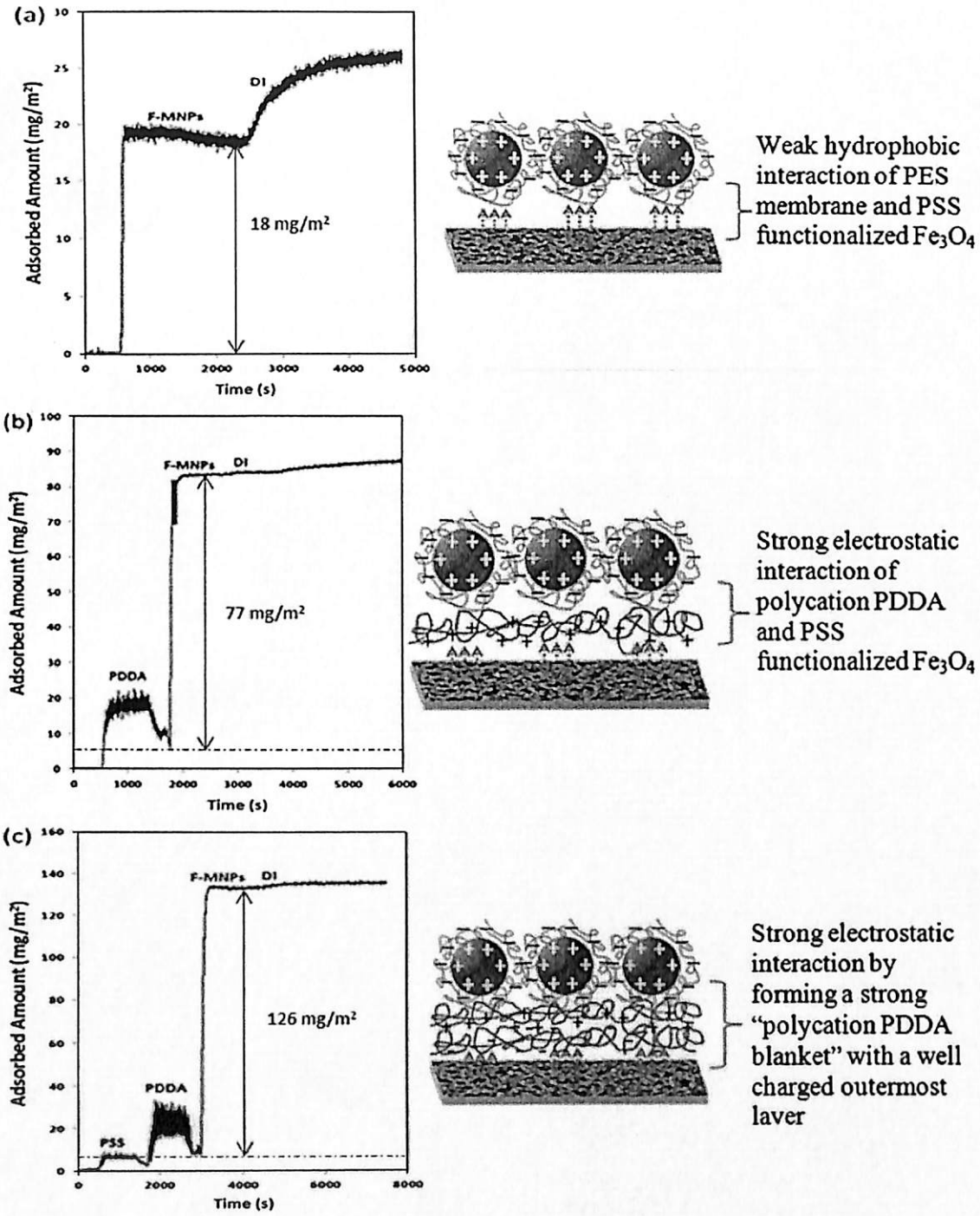

Fig. 5. Amount of F-MNPs (dispersed in DI water) adsorbed on a PES spin-coated quartz crystal sensor as a function of time at conditions (a) without precursor, (b) with a single layer coating of polycation PDDA, and (c) with a bilayer coating of polyanion PSS and polycation PDDA precursors.

PES membrane (Fig. 6a) was altered to a relatively rough surface for the magnetic responsive PES membrane (Fig. 6b). Homogenously distributed white dots (F-MNP colloids) were found on the membrane surface.

EDS analysis was used to confirm the existence of Fe_3O_4 on the magnetic responsive PES membrane. As shown in Fig. 6, Fe-element was not detectable on surface of the neat PES membrane but detected on surface of the magnetic responsive PES–Fe_3O_4 membrane. 0.22 Fe-at.% was found on the membrane surface (Fig. 6b) but only 0.06 Fe-at.% was discovered when scanned through the membrane cross sectional area (Fig. 7b, spectrum area 1 that representing the composite layer). These findings have confirmed that the F-MNPs were not penetrated into the substructure of MF membrane, but well distributed on surface of the thin composite layer. In fact, the homogenous distribution of these Fe_3O_4 (Fig. 6) on the membrane surface are believed to help in aligning the magnetic responsive F-MNPs in the same direction when an external magnetic field is applied. Magneto-induced rotation motions were induced when opposing magnetic field were alternately applied. This magneto-induced rotation further promotes

(a)

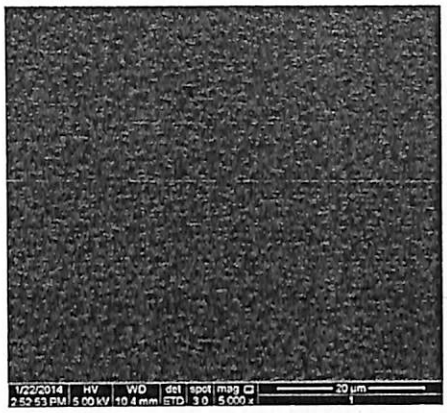

Element	Weight (%)	Atomic (%)
C	68.34	78.09
O	19.44	16.68
S	12.22	5.23
Fe	0.00	0.00

(b)

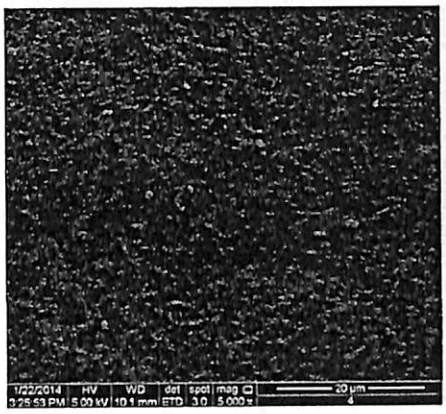

Element	Weight (%)	Atomic (%)
C	67.16	77.42
O	19.72	17.07
S	12.25	5.29
Fe	0.87	0.22

Fig. 6. FESEM micrograph and EDS results for top surface of (a) a neat PES membrane and (b) a magnetic responsive PES–Fe_3O_4 membrane.

(a)

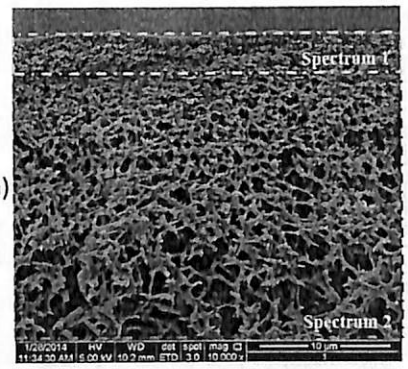

Element	Spectrum 1		Spectrum 2	
	Weight (%)	Atomic (%)	Weight (%)	Atomic (%)
C	68.00	75.40	69.26	77.48
O	27.13	22.57	22.91	19.24
S	4.87	2.03	7.84	3.28
Fe	0.00	0.00	0.00	0.00

(b)

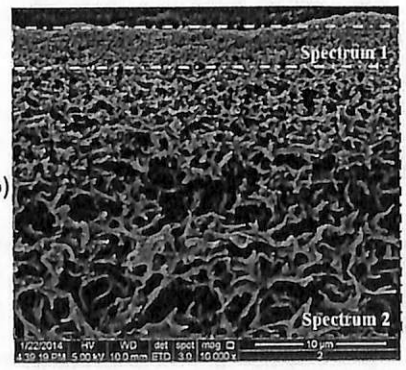

Element	Spectrum 1		Spectrum 2	
	Weight (%)	Atomic (%)	Weight (%)	Atomic (%)
C	68.63	77.12	67.47	78.24
O	23.05	19.42	17.50	15.23
S	8.06	3.4	15.03	6.53
Fe	0.26	0.06	0.00	0.00

Fig. 7. FESEM micrograph and EDS results for cross section of (a) a neat PES membrane and (b) a magnetic responsive PES–Fe_3O_4 membrane.

the magnetophoretic actuation of the F-MNP colloids, promoting the detachment of humic acid foulants from the membrane surface.

The membrane filtration performances were evaluated by the separation of HA foulants from the aqueous feed solution. The extent of membrane fouling was observed for the (1) neat PES

membrane without magnetophoretic rotation, (2) neat PES membrane with magnetophoretic rotation, (3) magnetic responsive PES–Fe_3O_4 membrane without magnetophoretic rotation and (4) magnetic responsive PES–Fe_3O_4 membrane with magnetophoretic rotation. As shown in Fig. 8, the neat PES membranes with or without magnetophoretic rotation was significantly fouled after 12 h of filtration. The filtrate flux for both neat membranes was reduced to approximately 48% of the initial flux. This fouling was due to a concentrated polarization resulting from agglomerated clusters of HA on the surface of the nearly neutrally charged porous PES matrix. In contrast, the PES–Fe_3O_4 membrane without magnetophoretic rotation showed a better antifouling capacity compared with the neat PES membrane. The membrane was also superior in the filtration flux, where the permeation after 12 h declined to approximately 57% of the initial flux. The observed better antifouling properties for the PES–Fe_3O_4 membrane were attributed to the end-capped F-MNP composite layer. The additional magnetic composite film increased both the negatively charged density and hydrophilicity of the PES membrane, making them less susceptible to fouling.

By introducing the magneto-induced rotation motion, the magnetic responsive PES–Fe_3O_4 membrane showed excellent antifouling ability. With the presence of magnetophoretic actuation of the Fe_3O_4 at the top magnetic composite layer, the filtrate flux was 72% of the initial flux after the same testing period of 12 h. Because of the existence of the magnetite colloids (Fe_3O_4) on the membrane surface, the negatively charged and hydrophilic modified PES–Fe_3O_4 membrane, which was originally susceptible to the fouling, showed greater resistance to fouling because of the externally applied magnetic field and subsequent actuation of the magnetic nano-colloids. This is an important and significant result that shows the antifouling capacity of the magnetic responsive PES–Fe_3O_4 membrane. The magnetophoretic actuation mode imposes a torque around the colloid. This induces a twisting effect on the magnetic nano-colloids that promotes the detachment of foulants from the membrane. This detachment assists in reducing the polarization concentration on the membrane surface and prolongs the life-span of the membrane.

QCM-D was used to quantitatively determine the mass interactions between the HA foulants and the membrane surface. The HA mass adsorbed (Fig. 9) was calculated using the Sauerbrey equation based on the QCM-D measurement data. The amount of HA

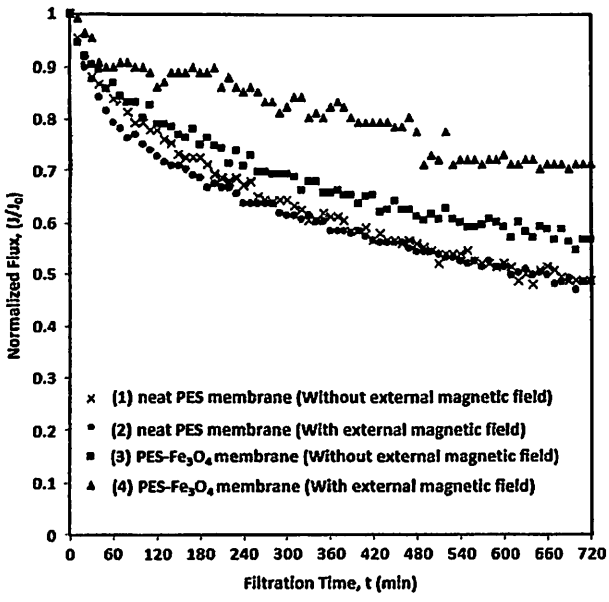

Fig. 8. Normalized filtrate flux for the filtration of 50 mg/L solutions of HA on the membrane fouling process.

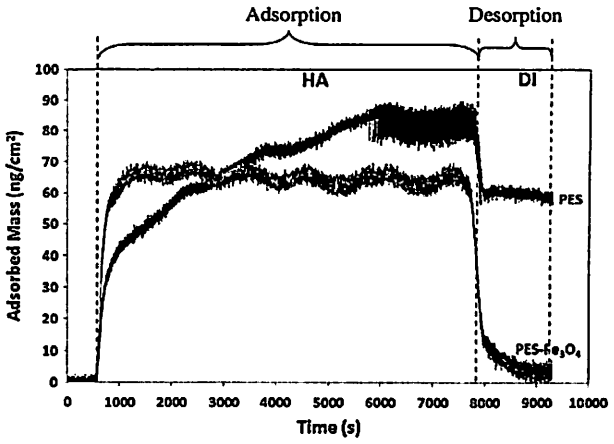

Fig. 9. Adsorption and desorption of HA on a modified PES–Fe_3O_4 and an unmodified neat PES membranes as a function of time.

adsorbed on the neat PES membrane (approximately 85 ng/cm^2) was slightly higher than that on the PES–Fe_3O_4 membrane (approximately 63 ng/cm^2). This result may be due to the increased negative charge density and hydrophilicity properties of the thin film Fe_3O_4 composite layer that makes the membrane less vulnerable to fouling. In Fig. 9, a wavy curve was observed when the HA solution was perfused across the PES–Fe_3O_4 membrane. It is suspected that there is a simultaneous adsorption and desorption of HA molecules at the membrane surface. As discussed earlier, only weakly interacting forces exist between the HA foulant and the modified PES–Fe_3O_4 membrane due to the electrostatic repulsion and hydrophilicity properties of the membrane. This could explain the weak deposition of HA molecules (less susceptible to fouling) on the modified PES–Fe_3O_4 membrane (Fig. 8). The initial fouling on the surface of the PES–Fe_3O_4 membrane could be due to the rough surface of the membrane. This rough surface may increase the absolute surface area for foulants to adhere to.

This observation (weak attachment of HA molecules to the membrane surface) was investigated by DI water washing steps. The cleaning efficiency for HA molecules attached to the PES–Fe_3O_4 membrane was excellent (approximately 96% of HA molecules were detached) compared with that of the neat PES membrane (approximately 34% of HA molecules were removed). This explains the stronger hydrophobic–hydrophobic interaction of the HA molecules with the neat PES membrane compared with the weak interaction existing between HA molecules and the electrostatic repulsion of the PES–Fe_3O_4 membrane, as explained earlier.

In terms of rejection performance, the PES–Fe_3O_4 membrane showed a relatively higher rejection (81%) compared with that of

Table 2
HA rejections after 12 h humic acid-fed microfiltration at 50 ppm HA feed solution adjusted to pH8.

	Rejection, R (%)	
	Average	Standard deviation
(1) Neat PES membrane (without external magnetic field)	74.97	0.29
(2) Neat PES membrane (with external magnetic field)	74.93	0.85
(3) PES–Fe_3O_4 membrane (without external magnetic field)	77.18	0.24
(4) PES–Fe_3O_4 membrane (with external magnetic field)	80.92	0.72

the neat PES membrane (75%, Table 2). The presence of F-MNPs capped to the membrane surface increased the surface negative charge that created an electrostatic repulsion between the charge moieties on F-MNPs and HA. The end-capped F-MNPs on the membrane surface likely constricted the membrane pores, resulting in narrow pore size distribution at the membrane surface, which contributed to higher HA rejection. In regards, the integration of the magnetite colloids into the membrane surface showed greatest mitigation effect towards the membrane fouling without compromising the rejection performance.

4. Conclusion

Fe_3O_4 functionalized by PSS was successfully end-capped to PES membranes with the precursor polyelectrolytes PSS and PDDA present between the functional F-MNP layer and the supporting PES membrane. In this study, the magnetophoretic actuations of Fe_3O_4 colloids deposited on the surface of the PES–Fe_3O_4 membranes were evaluated for the potent antifouling behavior. The presence of the hydrophilic and magnetophoretic characteristics of the Fe_3O_4 functional layer showed a significant reduction of membrane fouling by humic acid. The QCM-D results also demonstrated a good interaction between the F-MNP colloids and PES membrane in the presence of the polyelectrolytes PSS and PDDA. The overall filtration performance of this magnetic responsive PES–Fe_3O_4 membrane demonstrated an excellent permeation that suppressed membrane fouling (maintained at approximately 72% of the initial flux after 12 h of filtration) with a rejection performance of up to 81%. The reduced membrane fouling was due to the existence of the actuation motions of Fe_3O_4 nano-colloid under an oscillating external magnetic field which exposed to a twisting effect, promoting the detachment of HA from the membrane surface.

Acknowledgements

The authors wish to thank the financial support granted by The Institution of Higher Education FRGS Grant (6071251) and International Foundation for Science (IFS), Sweden (Grant No. 304/PJKIMIA/6050232). All authors are affiliated to the Membrane Science and Technology Cluster of USM. Q.H. Ng is financially assisted by Ministry of Higher Education (MOHE) and Universiti Malaysia Perlis (UniMAP).

References

[1] X. Jian, Y. Dai, G. He, G. Chen, Preparation of UF and NF poly (phthalazine ether sulfone ketone) membranes for high temperature application, J. Membr. Sci. 161 (1999) 185–191.
[2] P.D. Peeva, A.E. Palupi, M. Ulbricht, Ultrafiltration of humic acid solutions through unmodified and surface functionalized low-fouling polyethersulfone membranes – effects of feed properties, molecular weight cut-off and membrane chemistry on fouling behavior and cleanability, Sep. Purif. Technol. 81 (2011) 124–133.
[3] T. Zayas, V. Rómero, L. Salgado, M. Meraz, U. Morales, Applicability of coagulation/flocculation and electrochemical processes to the purification of biologically treated vinasse effluent, Sep. Purif. Technol. 57 (2007) 270–276.
[4] Z. Liang, Y. Wang, Y. Zhou, H. Liu, Z. Wu, Variables affecting melanoidins removal from molasses wastewater by coagulation/flocculation, Sep. Purif. Technol. 68 (2009) 382–389.
[5] R.W. Baker, Membrane Technology and Applications, second ed., John Wiley & Sons, Ltd., 2004.
[6] Y. Kouwonou, R. Malaisamy, K.L. Jones, Modification of PES membrane: reduction of biofouling and improved flux recovery, Sep. Sci. Technol. 43 (2008) 4099–4112.
[7] F. Diagne, R. Malaisamy, V. Boddie, R.D. Holbrook, B. Eribo, K.L. Jones, Polyelectrolyte and silver nanoparticle modification of microfiltration membranes to mitigate organic and bacterial fouling, Environ. Sci. Technol. 46 (2012) 4025–4033.
[8] Z. Wang, Y. Zhao, J. Wang, S. Wang, Studies on nanofiltration membrane fouling in the treatment of water solutions containing humic acids, Desalination 178 (2005) 171–178.
[9] H. Yamamura, S. Chae, K. Kimura, Y. Watanabe, Transition in fouling mechanism in microfiltration of a surface water, Water Res. 41 (2007) 3812–3822.
[10] C.Y. Tang, Y.N. Kwon, J.O. Leckie, The role of foulant–foulant electrostatic interaction on limiting flux for RO and NF membranes during humic acid fouling – theoretical basis, experimental evidence, and AFM interaction force measurement, J. Membr. Sci. 326 (2009) 526–532.
[11] M.A. Zazouli, S. Nasseri, M. Ulbricht, Fouling effects of humic and alginic acids in nanofiltration and influence of solution composition, Desalination 250 (2010) 688–692.
[12] S. Hong, M. Elimelech, Chemical and physical aspects of natural organic matter (NOM) fouling of nanofiltration membranes, J. Membr. Sci. 132 (1997) 159–181.
[13] P.D. Peeva, T. Pieper, M. Ulbricht, Tuning the ultrafiltration properties of antifouling thin-layer hydrogel polyethersulfone composite membranes by suited crosslinker monomers and photo-grafting conditions, J. Membr. Sci. 362 (2010) 560–568.
[14] G.N.B. Baroña, B.J. Cha, B. Jung, Negatively charged poly(vinylidene fluoride) microfiltration membranes by sulfonation, J. Membr. Sci. 290 (2007) 46–54.
[15] R. Malaisamy, A. Talla-Nwafo, K.L. Jones, Polyelectrolyte modification of nanofiltration membrane for selective removal of monovalent anions, Sep. Purif. Technol. 77 (2011) 367–374.
[16] K. Akamatsu, T. Furue, F. Han, S.-I. Nakao, Plasma graft polymerization to develop low-fouling membranes grafted with poly(2-methoxyethylacrylate), Sep. Purif. Technol. 102 (2013) 157–162.
[17] W. Zhang, G. He, P. Gao, G. Chen, Development and characterization of composite nanofiltration membranes and their application in concentration of antibiotics, Sep. Purif. Technol. 30 (2003) 27–35.
[18] C. Mbareck, Q.T. Nguyen, O.T. Alaoui, D. Barillier, Elaboration, characterization and application of polysulfone and polyacrylic acid blends as ultrafiltration membranes for removal of some heavy metals from water, J. Hazard. Mater. 171 (2009) 93–101.
[19] J. Kim, B. Van Der Bruggen, The use of nanoparticles in polymeric and ceramic membrane structures: review of manufacturing procedures and performance improvement for water treatment, Environ. Pollut. 158 (2010) 2335–2349.
[20] M. Namvar-Mahboub, M. Pakizeh, Development of a novel thin film composite membrane by interfacial polymerization on polyetherimide/modified SiO_2 support for organic solvent nanofiltration, Sep. Purif. Technol. 119 (2013) 35–45.
[21] H. Zhao, H. Li, H. Yu, H. Chang, X. Quan, S. Chen, CNTs–TiO_2/Al_2O_3 composite membrane with a photocatalytic function: fabrication and energetic performance in water treatment, Sep. Purif. Technol. 116 (2013) 360–365.
[22] R. Jamshidi Gohari, W.J. Lau, T. Matsuura, A.F. Ismail, Fabrication and characterization of novel PES/Fe–Mn binary oxide UF mixed matrix membrane for adsorptive removal of As(III) from contaminated water solution, Sep. Purif. Technol. 118 (2013) 64–72.
[23] Y. Liu, A. Wang, R.O. Claus, Layer-by-layer electrostatic self-assembly of nanoscale Fe_3O_4 particles and polyimide precursor on silicon and silica surfaces, Appl. Phys. Lett. 71 (1997) 2265–2267.
[24] J.S. Taurozzi, H. Arul, V.Z. Bosak, A.F. Burban, T.C. Voice, M.L. Bruening, V.V. Tarabara, Effect of filler incorporation route on the properties of polysulfone–silver nanocomposite membranes of different porosities, J. Membr. Sci. 325 (2008) 58–68.
[25] C. Schlemmer, W. Betz, B. Berchtold, J. Rühe, S. Santer, The design of thin polymer membranes filled with magnetic particles on a microstructured silicon surface, Nanotechnology 20 (2009).
[26] P. Jian, H. Yahui, W. Yang, L. Linlin, Preparation of polysulfone–Fe_3O_4 composite ultrafiltration membrane and its behavior in magnetic field, J. Membr. Sci. 284 (2006) 9–16.
[27] R. Wang, Y. Chen, H. Xie, G. Kai, Z. Wang, J. Pan, Polysaccharide separation mechanism in polysulfone–Fe_3O_4 magnetic composite membranes, Chin. Sci. Bull. 56 (2011) 1951–1956.
[28] K.L. Chen, M. Elimelech, Aggregation and deposition kinetics of fullerene (C60) nanoparticles, Langmuir 22 (2006) 10994–11001.
[29] D. Xu, C. Hodges, Y. Ding, S. Biggs, A. Brooker, D. York, Adsorption kinetics of laponite and ludox silica nanoparticles onto a deposited poly(diallyldimethylammonium chloride) layer measured by a quartz crystal microbalance and optical reflectometry, Langmuir 26 (2010) 18105–18112.
[30] E. Arkhangelsky, F. Wicaksana, C. Tang, A.A. Al-Rabiah, S.M. Al-Zahrani, R. Wang, Combined organic–inorganic fouling of forward osmosis hollow fiber membranes, Water Res. 46 (2012) 6329–6338.
[31] A.E. Contreras, Z. Steiner, J. Miao, R. Kasher, Q. Li, Studying the role of common membrane surface functionalities on adsorption and cleaning of organic foulants using QCM-D, Environ. Sci. Technol. 45 (2011) 6309–6315.
[32] M. Hashino, K. Hirami, T. Katagiri, N. Kubota, Y. Ohmukai, T. Ishigami, T. Maruyama, H. Matsuyama, Effects of three natural organic matter types on cellulose acetate butyrate microfiltration membrane fouling, J. Membr. Sci. 379 (2011) 233–238.
[33] G. Sauerbrey, Verwendung von Schwingquarzen zur Wägung dünner Schichten und zur Mikrowägung, Z. Phys. 155 (1959) 206–222.
[34] G. Liu, D.M. Dotzauer, M.L. Bruening, Ion-exchange membranes prepared using layer-by-layer polyelectrolyte deposition, J. Membr. Sci. 354 (2010) 198–205.
[35] F. Hua, Y.M. Lvov, Layer-by-layer assembly, in: E. Victor, R. Manoj Kumar, M.K.R. Ozlem Yavuz, Victor Erokhin, Y. Ozlem (Eds.), The New Frontiers of Organic and Composite Nanotechnology, Elsevier, Amsterdam, 2008, pp. 1–44 (Chapter 1).

[36] T. Ishigami, K. Amano, A. Fujii, Y. Ohmukai, E. Kamio, T. Maruyama, H. Matsuyama, Fouling reduction of reverse osmosis membrane by surface modification via layer-by-layer assembly, Sep. Purif. Technol. 99 (2012) 1–7.
[37] M.D. Miller, M.L. Bruening, Correlation of the swelling and permeability of polyelectrolyte multilayer films, Chem. Mater. 17 (2005) 5375–5381.
[38] M. Kolasińska, P. Warszyński, The effect of support material and conditioning on wettability of PAH/PSS multilayer films, Bioelectrochemistry 66 (2005) 65–70.
[39] C. Picart, Polyelectrolyte multilayer film: from physico-chemical properties to the control of cellular processes, Curr. Med. Chem. 15 (2008) 685–697.

Chemical Engineering Journal 243 (2014) 68–78

Contents lists available at ScienceDirect

Chemical Engineering Journal

journal homepage: www.elsevier.com/locate/cej

Layer-by-layer assembly of iron oxide magnetic nanoparticles decorated silica colloid for water remediation

By Hui Xin Che [a], Swee Pin Yeap [a], Abdul Latif Ahmad [a], JitKang Lim [a,b,*]

[a] School of Chemical Engineering, Universiti Sains Malaysia, Nibong Tebal, Penang 14300, Malaysia
[b] Department of Physics, Carnegie Mellon University, Pittsburgh, PA 15213, USA

HIGHLIGHTS

- Layer-by-layer assembly of magnetic nanoparticles, polyelectrolyte and silica colloid nanocomposite.
- Nanocomposite with good colloidal stability, exhibits magnetic and catalytic bifunctionalities.
- Catalytic degradation dominates over electrostatic interactions for dye removal.
- Nanocomposite remained catalytically active after 6 months of storage.

GRAPHICAL ABSTRACT

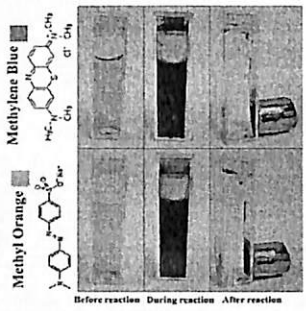

ARTICLE INFO

Article history:
Received 12 November 2013
Received in revised form 27 December 2013
Accepted 30 December 2013
Available online 8 January 2014

Keywords:
Nanocomposite
Electrostatic interaction
Colloidal stability
Magnetic nanoparticle
Catalytic property
Water remediation

ABSTRACT

Silica colloid–polyelectrolyte–iron oxide nanocomposite with both magnetic and catalytic properties has been synthesized via layer-by-layer assembly. Dynamic light scattering (DLS) and electrophoretic mobility measurements were employed to monitor the evolution of these structures from silica colloid to silica colloid–polyelectrolyte–iron oxide composite. In addition to DLS, transmission electron microscope was used to investigate the morphology of nanostructure synthesized at each stage. The final structure formed show good colloidal and catalytic stability and real time magnetophoretic response under low magnetic field gradient. Here we demonstrated the potential environmental engineering application of this nanocomposite by taking organic dye, Methylene Blue (MB) and Methyl Orange (MO), as our model system. The experiment was conducted by testing the capability of nanomaterials synthesized at each stage, namely silica colloid, polyelectrolyte-functionalized silica colloid (silica–PDDA), and silica colloid–polyelectrolyte–iron oxide composite (silica–PDDA–IOMNPs), for dye removal. By taking into account the electrostatic interactions between the dye molecules and the as-synthesized nanomaterials, we verified that silica colloid–polyelectrolyte–iron oxide composite is superior for pollutant removal from aqueous environment mainly due to its catalytic property. We rationalized our finding by performing (1) Langmuir and Freundlich adsorption analysis, and, (2) pseudo-first-order and pseudo-second-order kinetic study for all three species of aforementioned nanomaterials. The reusability of silica–PDDA–IOMNPs nanocomposite was tested by subjecting this nanomaterial for multiple cycle of dye removal process. This hybrid material remained catalytically active after six months of storage.

* Corresponding author. Address: School of Chemical Engineering, Engineering Campus, Universiti Sains Malaysia, Seri Ampangan, 14300 Nibong Tebal, Penang, Malaysia. Tel.: +60 4 599 6423; fax: +60 4 599 1013.
E-mail address: chjitkangl@eng.usm.my (J. Lim).

1385-8947/$ - see front matter © 2014 Elsevier B.V. All rights reserved.
http://dx.doi.org/10.1016/j.cej.2013.12.095

1. Introduction

Magnetic nanoparticle has been used extensively for biological [1–4] and environmental [5,6] applications mainly due to its unique catalytic and magnetic properties with extremely high surface-to-volume ratio [6]. Iron oxide magnetic nanoparticles (IOMNPs) are sometimes used solely, without further modification, to remove heavy metals from industrial wastewater [7]. However, pure inorganic magnetic iron based nanoparticle can easily form large aggregate driven by inter-particles van der Waals and magnetic attractions, and hence negate the benefits associated to its nanoscopic dimension [8]. In addition, the nanotoxicity exhibited by IOMNPs [9] has also discouraged the large scale implementation of this nanomaterial for environment remediation. Therefore, surface modification of IOMNPs is necessary to promote colloidal stability of the particles suspension formed and also minimize nanotoxicity effect in order to enhance its functionality for targeted application [10]. The most popular way to achieve this target are either surface modified IOMNPs with organic [11,12] or inorganic material [13,14] or integrating the IOMNPs into polymeric matrix [15]. In former case, the IOMNPs remained as an individual particle, whereas in later scenario, the particles are artificially coagulated into loosely packed polymeric matrix. Nevertheless, in all these cases the IOMNPs retained both its magnetic and catalytic properties, which are crucial for environmental engineering related application. In this article, we proposed the assembly of IOMNPs with layer-by-layer approach [16] onto silica colloid which served as nanotemplate and use this nanostructure for water treatment purpose. Cationic polyelectrolyte was employed as binding agent to promote the attachment of IOMNPs onto the silica colloid. The final nanocomposite composed of silica colloid as the inner core coated with polyelectrolyte and IOMNPs as outer-shell.

There present numerous chemical routes for the synthesis and surface modification of silica colloid and all these aspects contribute to the versatile use of silica colloid for engineering applications [17]. Silica alone is widely used in water remediation [18,19] where it served as adsorbent to remove Basic Blue 3 and Astrazone Blue(Basic) dyes respectively from textile effluent. Moreover, surface functionalization of silica colloid by decorating its micro or meso-porous channels and/or the external particle surface with various functional groups has significantly enhanced its effectiveness for environmental application [20,21]. Combining silica colloid and IOMNPs into one unified nanostructure offers attractive architecture for water remediation. Silica is widely chosen as material to functionalize IOMNPs due to its stability, possible reuse and relative rapidity in reaching equilibrium, high mechanical resistance and high surface area [22]. Deposition of silica shells on IOMNPs has been successfully carried out by different procedures [23,24]. On the other hand, embedding IOMNPs into silica matrix for wastewater treatment by taking advantage of its high surface areas and pore volumes has also being developed [13]. But the direct deposition of iron compounds on silica template is much more difficult [25]. There were some studies about the method of repetitive heterocoagulation to synthesize composite of silica core-repetitive magnetic/silica-shell [26] and developing Fe_3O_4 nanoparticle/polyelectrolyte multilayer assembly on colloidal silica [27].

Even though the design and synthesis of silica-core with magnetic-shell composite has been widely discussed in literature, to best of our knowledge, there are no any illustrations about the environmental engineering application of this composite material. There are several advantages to incorporate the IOMNPs onto silica colloid. Firstly, due to the cooperative nature of the magnetophoresis [28,29], these nanocomposite should be less susceptible to the thermal randomization energy compared to individual particle [30] and experienced much greater magnetophoretic force to overcome the viscous drag [31,32]. These scenarios would enable rapid magnetic collection of nanocomposite which composed of magnetic particles clusters after their usages for water remediation. Furthermore, the confinement of IOMNPs onto the surface of silica colloid mitigates the particles aggregation problems and also reduces the direct exposure of IOMNPs to environment. Thus, lessen the nanotoxicity of IOMNPs associated to its small dimension [33]. In addition, since the IOMNPs are artificially immobilized onto the silica colloid with loosely bound polyelectrolyte matrix, we anticipated that the deprivation of catalytic active sites of IOMNPs can be minimized. Subsequently, this open matrix structure allows the full utilization of catalytic capability of the nanocomposite formed for degradation of targeted pollutants.

In this work, positively charged Methylene Blue (MB) and negatively charged Methyl Orange (MO) dyes are chosen as modeled pollutants to test the aptitude of our as-synthesized silica colloid–polyelectrolyte–iron oxide composite for water remediation. In addition to ease of detection by colorimetric method, both MB and MO were selected as our model system due to their similarity in molecular structure (Fig. 1) and, obvious charge differences. By having very similar molecular structure, both MB and MO molecules would have comparable transportation behaviors. This feature allowed us to neglect the differences associated to their transport properties while comparing separation efficiency of these molecules in our dye removal experiments. Whereas, the charge differences between MB and MO provide us a unique opportunity to test the critical role of electrostatic interactions for pollutant removal by the silica colloid–polyelectrolyte–iron oxide composite via adsorption and catalytic degradation. We anticipated that electrostatic interaction would have much adverse effect on the former mechanism and is less influential on the latter case. In addition, MB and/or MO have been widely used in textile, printing, food, and pharmaceutical industries [34,35], and hence, industrial effluents containing these molecules need to be treated effectively to prevent further deterioration of our water resources. By investigating the feasibility of synthesized nanoparticles in dyes removal, the degradation of other organic pollutants from contaminated water can be readily carried out by using advanced oxidation process in this heterogeneous catalytic reaction system. In fact, the advanced oxidation process [36] is a promising method which has been used in various emerging heterogeneous Fenton system to treat contaminants in wastewater, for example colorants [37–40], herbicide [41], insecticide [42] as well as pharmaceutical waste [43,44].

2. Materials and methods

2.1. Materials

All the reagents employed in this work were of analytical grade and used as received without further purification. Ethanol

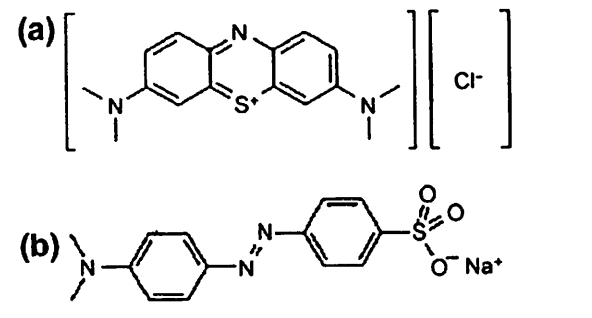

Fig. 1. The structural formula for (a) positively charged Methylene Blue (MB) and (b) negatively charged Methyl Orange (MO).

(absolute) and Hydrogen peroxide (H_2O_2, 100 volumes >30%w/v) were obtained from Fisher Scientific (M) Sdn. Bhd. Ammonia solution (25%), Methylene Blue (MB, 319.86 g/mole) and Methyl Orange (MO, 327.34 g/mole) were supplied by Merck. Tetraethylorthosilicate, (TEOS, 98%) was purchased from Acros Organics. Poly(diallyldimethylammonium chloride), (PDDA, low molecular weight with average molecular weight, $M_w \sim 100{,}000$–200,000 and 20 wt% in water) was purchased from Aldrich Chemistry. Iron oxide nanopowder (Fe_3O_4, 20–30 nm, 98 + % purity) was obtained from Nanostructured & Amorphous Materials Inc. In all experiments, deionized water was employed from Purelab Option-Q with resistivity at 18 MΩ cm from a potable water source.

2.2. Preparation of silica colloid–polyelectrolyte–iron oxide composite

The pictorial representation of major steps involved in silica colloid–polyelectrolyte–iron oxide composite synthesis was shown in Fig. 2.

2.2.1. Synthesis of silica colloids

Submicron sized, monodispersed silica colloids were synthesized via modified *Stöber process* [45] to serve as a submicron template for the assembly of surface functionalized IOMNPs via layer-by-layer assembly with the introduction of polyelectrolyte layer(s) between them. In this method, ethanol, tetraethoxyorthosilicate and ammonia with ratio 30:1:3 were mixed and the reaction mixture was allowed to magnetically stir continuously for 2 h. At the end of reaction time, the initial colorless reaction mixture turned milky and the silica colloids were obtained as sediment by centrifugation at 3500*g* for 25 min to remove the excess reactants (see Fig. S1(a) in Supporting Information). The silica colloids were redispersed in deionized water and were centrifuged again with the same speed for 3 times in order to get pure silica nanoparticles before suspending in 1.0 mM NaCl solution.

2.2.2. Synthesis of polyelectrolyte-functionalized silica colloids

Since silica colloids are negatively charged with zeta potential of −65.3 mV, cationic PDDA was introduced to decorate silica colloids surface and promote charge reversal. For PDDA attachment, initially 0.01 g/mL of PDDA solution was prepared and was ultrasonicated for at least 60 min to assist their dissolution as well as to promote good dispersity of the polyelectrolyte solution. The PDDA concentration is chosen to make sure the available polyelectrolyte molecules are at least 500 times excess the estimated amount needed to form monolayer on the silica surface. Later silica colloids were added in the PDDA solution in mass ratio of 1:7.5 under intense ultrasonication. The mixture was left overnight on an end-to-end rotator mixer with rotational speed at 40 rpm to promote full attachment of the PDDA onto silica colloids. Then, the polyelectrolyte-functionalized silica colloids were separated out as white precipitate from the solution after subjected to centrifugation at 3500*g* for 25 min (see Fig. S1(b) in Supporting Information). The nanoparticles obtained went through three repeated deionized water redispersion/centrifugation cycles in order to get pure polyelectrolyte-functionalized silica colloids before transfer to 1.0 mM NaCl solution.

2.2.3. Synthesis of silica colloid–polyelectrolyte–iron oxide composite

The silica colloid–polyelectrolyte–iron oxide composite was fabricated by using purchased IOMNPs. The ratio of IOMNPs weight to PDDA-coated silica nanoparticles surface area was approximately 126.29 mg/m^2. Later, 1.0 mL of 0.01 g/mL polyelectrolyte-functionalized silica colloids was added drop-by-drop into 500.0 mL IOMNPs solution and this process was carried out under sonication in order to maximize the dispersity of IOMNPs. The mixture was then transferred to centrifuged tubes and left for 1 day on an end-to-end rotator mixer with rotational speed at 40 rpm. This step is necessary to promote full attachment of the negatively charged IOMNPs onto the polyelectrolyte-functionalized silica colloids. The silica–polyelectrolyte–iron oxide nanocomposite formed was collected by centrifugation at 10,000*g* for 10 min. The retantate was dispersed into deionized water by ultrasonication. For full removal of freely suspended IOMNPs, this centrifugation and washing steps were repeated for 2 more times. As a result, a novel silica–polyelectrolyte–iron oxide nanocomposite exhibiting catalytic and magnetic bifunctionalities was obtained.

2.3. Decolorization experiments

The stock solution for MB and MO were first prepared at the concentration of 10,000 mg/L. Depends on the need of each experiment, the working concentration were obtained by dilution using deionized water. The decolorization experiments were carried out using nanoparticles synthesized at each stage, namely silica colloids, polyelectrolyte-functionalized silica colloid (silica–PDDA) and silica colloid–polyelectrolyte–iron oxide nanocomposite (silica–PDDA–IOMNPs nanocomposite). In this work, all the experiments were conducted by adding 1.0 mL of silica colloid and silica–PDDA with concentration at 0.01 g/mL to 9.0 mL dyes solution whereas 1.0 mL of 0.01 g/mL silica–PDDA–IOMNPs nanocomposite was added to solution containing 0.5 mL of H_2O_2 and 8.5 mL of dyes solution in order to make up the right particle concentration. It is worth to note that there is no pH control was performed during the decolorization experiment. With the presence of H_2O_2, the reaction mixture was in the pH range of 6.47–6.56. The solution pH would influence the degradation kinetic of the dyes molecules [46,47], conformation change of the PDDA network [48,49] and also the surface charge of the IOMNPs [50,51]. Hence,

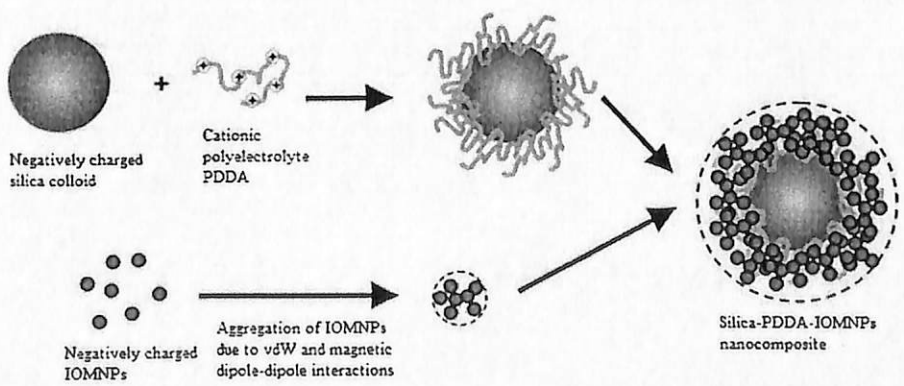

Fig. 2. Schematic diagram showing the major steps involved in layer-by-layer assembly of silica–PDDA–IOMNPs nanocomposite.

the role of pH in dictating the removal mechanism is a complex interplay of these three factors. The mixture was placed in a capped glass vial and left on an end-to-end rotator mixer with rotational speed at 40 rpm. Upon the completion of each experiment, for non-magnetic particle suspension, such as silica and silica–PDDA, centrifugation at 3500g were conducted to separate the particles out from the suspension. Whereas, for silica–PDDA–IOMNPs nanocomposite, a neodymium boron ferrite (NdBFe) cylindrical magnet with surface magnetization at ~6000 Gauss (Ningbo YuXiang E&M Int'l Co., Ltd.) was employed to harvest the particles out from the suspension. The time dependent magnetophoresis curve of silica–PDDA–IOMNPs nanocomposite under the influence of NdBFe magnet was evaluated before and after the decolorization work. Fig. S2 in Supporting Information revealed that the nanocomposite remained magnetically responsive after the usage and registered similar magnetophoretic collection rate and time. The remaining concentration of dye in the supernatant was determined calorimetrically with solution depletion method.

2.4. Measurement of dye concentration

The absorbance of dyes was analyzed using UV–vis spectrophotometer (Shimadzu Company, UVmini-1240) with the maximum absorbance wavelength, λ_{max} for MB at 666 nm and for MO at 480 nm. Prior to the measurement, calibration curves were constructed by using the standard MB and MO solution with a known concentration to obtain absorbance-concentration profile. The instant concentration of dyes in the reaction mixture at different reaction times was determined by measuring the absorption intensity at respective wavelengths and with calibration curves.

The amount of dye adsorbed on nanoparticles at a predetermined time t, q_t (mg/g), was determined using solution depletion method with following equation:

$$q_t = \frac{(C_o - C_t)V}{m} \quad (1)$$

The dye removal percentage (η) can be calculated by the following equation:

$$\eta = \frac{(C_o - C_t)}{C_o} \times 100\% \quad (2)$$

where C_o and C_t is the dye concentration (mg/L), at initial and instant time, t (min), V is the volume of solution (L) and m is the mass of nanoparticles used (g).

2.5. Characterization of the synthesized nanoparticles

The size distributions of the nanostructures at each stages of synthesis were determined by dynamic light scattering (DLS) (Malvern Instruments, Zetasizer Nano-ZS). The CONTIN algorithm was employed to fit the light scattering intensity autocorrelation function to provide an intensity-weighted distribution of hydrodynamic diameter (see Table 1). By using the same analytical instrument, we measured the electrophoretic mobility of the silica colloid before and after surface modification. We then calculated the zeta potential of the nanostructures formed at each stages of synthesis in 1.0 mM NaCl by Helmholtz–Smoluchowski limit (see Table 1). Transmission electron microscope (TEM) (JEOL, JEM-200CX) was employed to verify the structure evolution of the particles at different phases of synthesis (see Fig. 3).

Table 1
Zeta potential and hydrodynamic diameter of different nanoparticles measured by Zetasizer Nano-ZS (Malvern Instruments).

	Zeta potential (mV)	Hydrodynamic diameter (nm)
Silica colloids	−65.3	253.6 ± 1.59
Silica–PDDA	+58.3	277.5 ± 3.13
Cluster of IOMNPs	−6.6	297.6 ± 104.13
Silica–PDDA–IOMNPs	+25.8	392.9 ± 51.86

3. Results and discussion

3.1. Characterization of the synthesized nanoparticles

The morphology of nanoparticles involved at each stage of silica–PDDA–IOMNPs nanocomposite synthesis was revealed by TEM (Fig. 3). As illustrated in Fig. 3a, the silica colloids are spherical in shape with polydispersity index of 0.016 and having an averaged diameter at around 260.9 ± 1.9 nm (comparable with hydrodynamic diameter of 253.6 ± 1.6 nm measured by DLS). Fig. 3b shows TEM micrograph of IOMNPs with diameter at around 20.0 ± 76.5 nm. However, the hydrodynamic diameter of IOMNPs measured by using DLS is 297.6 ± 104.1 nm. Therefore, the size mismatch observed for IOMNPs between the measured hydrodynamic diameter using DLS and the TEM image analysis suggested that the IOMNPs aggregated into small clusters when dispersing in the aqueous environment for DLS measurement. This is consistent with our previous observations, in which without surface modification, electrostatic repulsion alone is insufficient to overcome the flocculation inducing forces, such as van der Waals and magnetic dipole–dipole interactions between the IOMNPs [31]. Under this scenario, the attachment of IOMNPs onto silica colloids need to be carried out instantaneously after their full dispersion into the working media and the entire process should be conducted under intense sonication. Fig. 3c and Fig. 3d shows the physical appearance of silica–PDDA–IOMNPs nanocomposite after the attachment of IOMNPs. The inevitable clustering of IOMNPs due to van der Waals and magnetic forces on the surface of a silica–PDDA could be visualized in Fig. 3c. Due to the excessive wetting and drying nature of the silica–PDDA–IOMNPs nanocomposite on TEM grid, the particles looked aggregate extensively as shown in Fig. 3d.

In all cases, we prolonged DLS monitoring on these silica–PDDA–IOMNPs nanocomposite and bare IOMNPs at 10.0 mg/L to compare the colloidal stability of these two suspensions (Fig. 4), individual IOMNPs flocculated into large clusters in aqueous solution. Initially, the bare IOMNPs appeared as small clusters with average hydrodynamic diameter of 245.3 nm and the clusters continue to flocculate, forming larger clusters with higher hydrodynamic diameter. This flocculation tendency of the bare IOMNPs was attributed to both the long-range van der Waals and the magnetic attraction [45]. By construction of silica–PDDA–IOMNPs nanocomposite, the aggregation is mitigated and the colloidal stability is promoted. As seen from Fig. 4, the average hydrodynamic diameter of silica–PDDA–IOMNPs nanocomposite was almost constant over the entire time course of 5 h. In addition, the particle stability of nanocomposite in real-life environment was demonstrated by anticipating 1.0 mM NaCl and 10.0 mM NaCl as the background medium. In fact, the electrolyte condition of 1–10 mM NaCl indeed represents the groundwater condition [52]. From Fig. S3 in Supporting Information, nanocomposite retained colloidal stability even in high ionic strength environment.

As seen from Table 1, the synthesized silica colloids yield zeta potential of −65.3 mV in 1.0 mM NaCl. The presence of PDDA polyelectrolyte on the outmost layer of silica colloids caused a reversal of zeta potential to +58.3 mV. On top of that, the orientation of the adsorbed polyelectrolyte on silica particle surface is most probably appeared as trains, loops and tails which has been well-investigated by the Fleer's group [53,54]. This adsorbed layer of cationic PDDA serves as the binding agent to facilitate the attachment of

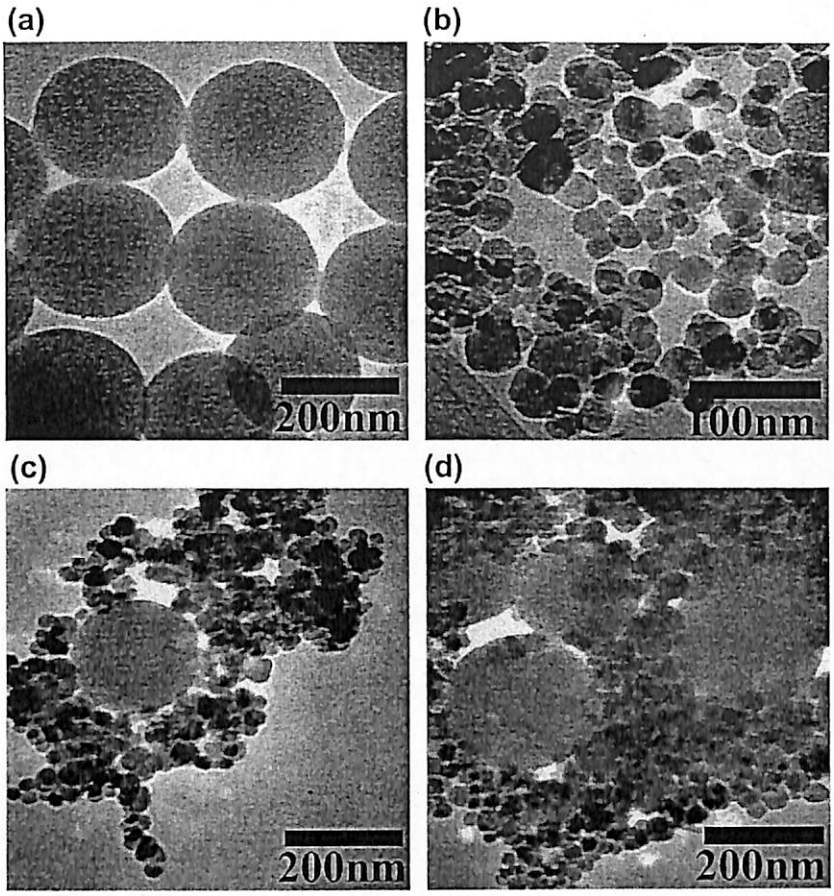

Fig. 3. TEM micrographs of (a) silica colloids, (b) IOMNPs and IOMNPs covered on (c) one and (d) four PDDA coated silica colloid.

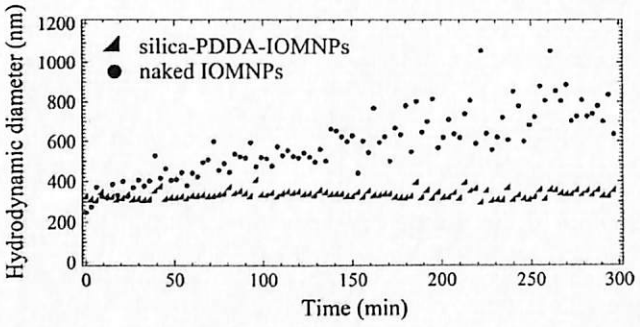

Fig. 4. Colloidal stability is conducted by studying the changing of averaged hydrodynamic diameter of silica–PDDA–IOMNPs nanocomposite and bare IOMNPs over predetermined time where the data were collected every 3 min for total 5 h run.

negatively charged IOMNPs with zeta potential at −6.6 mV. After silica–PDDA–IOMNPs nanocomposite was formed, the entire structure registered a positive zeta potential value at +25.8 mV even though the outmost area of this structure is occupied by negatively charged IOMNPs. This result indicated that IOMNPs have integrated into polyelectrolyte–silica matrix which subsequently suppressed the highly positive charged PDDA intermediate layer resulting in a net loss of zeta potential of silica–PDDA–IOMNPs nanocomposite from +58.3 mV to +25.8 mV. Thus, the drastic surface charge changes as observed at each stage of synthesis suggest successful attachment of PDDA and IOMNPs onto the silica colloid forming a three-layers-composite. The synthesized nanocomposite can be collected by external magnet in much more rapid manner than the bare IOMNPs as illustrated in Fig. 5. It can be seen from Fig. 5 that there was a rapid collection and obvious clearance of silica–PDDA–IOMNPs nanocomposite suspension within the first minute of magnetic separation, whereas the solution of bare IOMNPs was still remained as brownish suspension even after 4 min exposure to a permanent magnet. The snap shot shown in Fig. 5 is a perfect illustration of the magnetic superiority of nanocomposite over bare IOMNPs. Since in the nanocomposite, the IOMNPs are artificially assembled on the surface of silica colloid, the cooperative magnetophoretic force imposed on this structure is greater than the thermal randomization and viscous drag experienced by it [30].

3.2. Removal of MB and MO from aqueous environment

Concentration of MB and MO dyes at 5.0 mg/L was used to test our hypothesis of using silica, silica–PDDA and silica–PDDA–IOMNPs nanocomposite as dye decolourization agents. The temporal evolution of the dye removal efficiency of these three species of nanomaterial within two days was shown in Fig. 6.

Silica colloids, used as a nanotemplate for further construction of silica–PDDA–IOMNPs nanocomposite, exhibited negative surface charge which can be confirmed from the electrophoretic mobility measurement (Table 1). This highly negative charged silica colloids managed to remove positively charged MB with 86.64% efficiency (Fig. 6a and Fig. S1(c) in Supporting Information) compared to only 4.91% removal of negatively charged MO within the same time interval (Fig. 6b and Fig. S1(e) in Supporting Information). This observation is mainly due to the electrostatic interaction between the negatively charged silica colloids and dye components as illustrated in Fig. 7a. The large discrepancy of

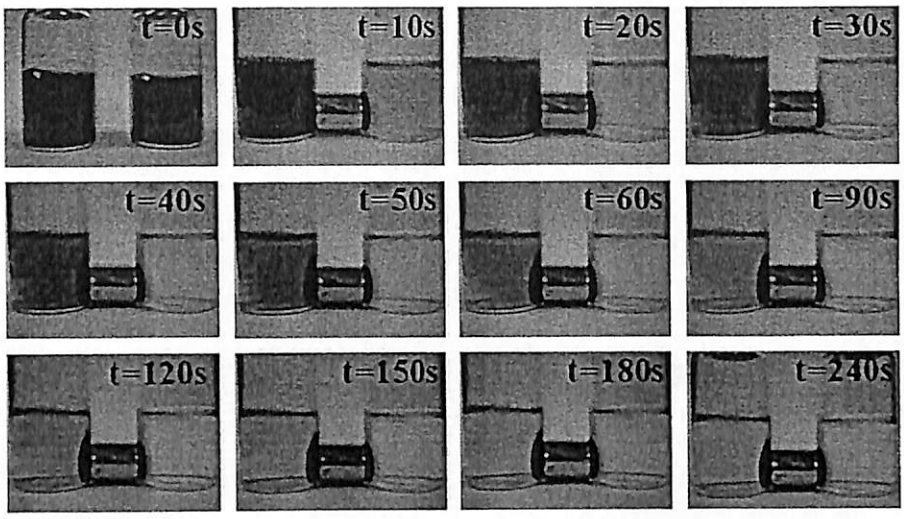

Fig. 5. Comparison the collection rate of (left) bare IOMNPs and (right) silica–PDDA–IOMNPs nanocomposite by a NdFeB magnet within 4 min. Both suspensions were prepared with concentration at 500 mg/L. The crystal clear solution formed at the end of magnetic collection for silica–PDDA–IOMNPs suspension also directly proved that both the silica colloid and IOMNPs have been integrated into one unified structure.

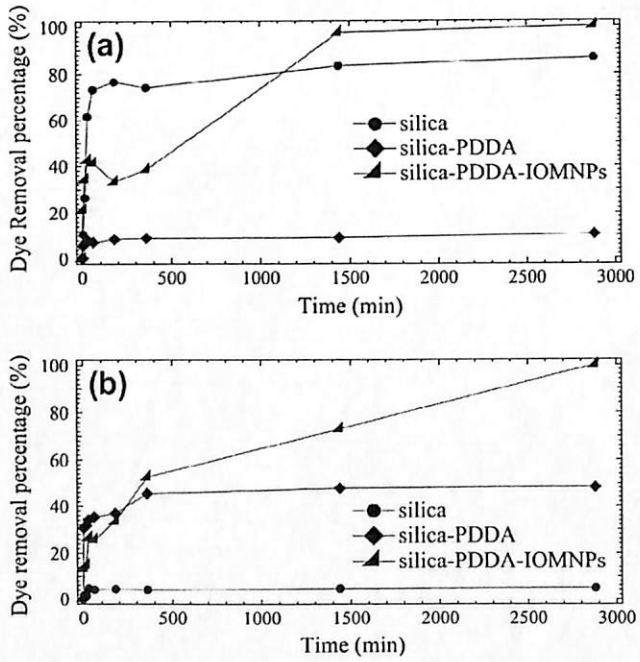

Fig. 6. Dye removal percentage of different as-synthesized nanoparticles used in (a) MB and (b) MO.

MB and MO removal by silica colloid suggested that electrostatic interaction plays an important role in dictating the adsorption-driven removal mechanism. Negatively charged silica colloids attracted and adsorbed positively charged MB but repelled MO with the same charge.

Silica colloids were then surface modified by the attachment of cationic PDDA. After the coating process, silica–PDDA turned out to be positively charged due to the outer PDDA shell formed on silica colloids. This highly charged silica–PDDA in turn can remove negatively charged MO (48.32%) (Fig. 6b and Fig. S1(f) in Supporting Information) better compared to MB (10.68%) (Fig. 6a and Fig. S1(d) in Supporting Information). Compared to the 86.64% removal of MB by oppositely charge silica colloids, there is only 48.32% removal of MO by silica–PDDA. We suspect that the underlying silica layer do play an important role in causing low percentage removal of MO by silica–PDDA structure. Even though there presents an extended layer of PDDA coating on the surface of silica colloid, as revealed by DLS measurement (see Table 1 for hydrodynamic diameter increment after PDDA attachment), this layer has limited capability to register oppositely charged MO into its matrix. The localized neutralization of charge after adsorption of MO onto PDDA layer(s) would cause the incoming MO to suffer higher resistant as the repulsion from underlying silica layer is more pronounced. This scenario is totally different from the case of MB adsorption onto bare silica colloid, in which the incoming MB can diffuse into mesoporous channel of silica and adsorbed on the inner surface of silica pore.

Apart from that, the removal of MB by silica–PDDA registered a none-zero value at 10.68% implied that, besides electrostatic, there is other interaction involved between MB and silica–PDDA even though they are both cationic. This observation lead us to believe hydrophobic interaction may also happened between hydrocarbon portion of dye molecule and non-polar part of PDDA [55]. Under this context, Seo and coworkers [56] discussed the contribution of electrostatic, hydrophobic and hydrogen bonding interaction on the sorption behavior of hydrogels and MO. In addition, Nandini and Vishalakshi [57] reported that reversal of metachromasy in MO-polyion complexes by adding alcohols/urea suggested the involvement of hydrophobic forces in polymer–dye interaction. As reported by both groups, the binding of dye molecules is primarily electrostatic force which is further reinforced by hydrophobic interaction. Therefore, the charge density and the flexibility of polyelectrolyte in terms of hydrophobicity of non-polar part and the bulkiness of the polar-part play vital role in polyelectrolyte–organic dye interaction. However, their work revealed that the electrostatic force is still the principal contributor to the dye removal. This is in consistent with our experiment results where the removal efficiency of MO (48.32%) is higher compared to MB (10.68%) by silica–PDDA.

Introduction of negatively charged IOMNPs into the positively charged silica–PDDA colloid has greatly suppressed the overall net surface charge of the final structure formed. At almost neutral pH, this silica–PDDA–IOMNPs nanocomposite exhibits a zeta potential value of +25.8 mV (as shown in Table 1). In this case, 100% removal of MB and MO was achieved by using silica–PDDA–IOMNPs nanocomposite (see Fig. 6) where at the end of the dye removal experiment, initial blue color of MB and orange

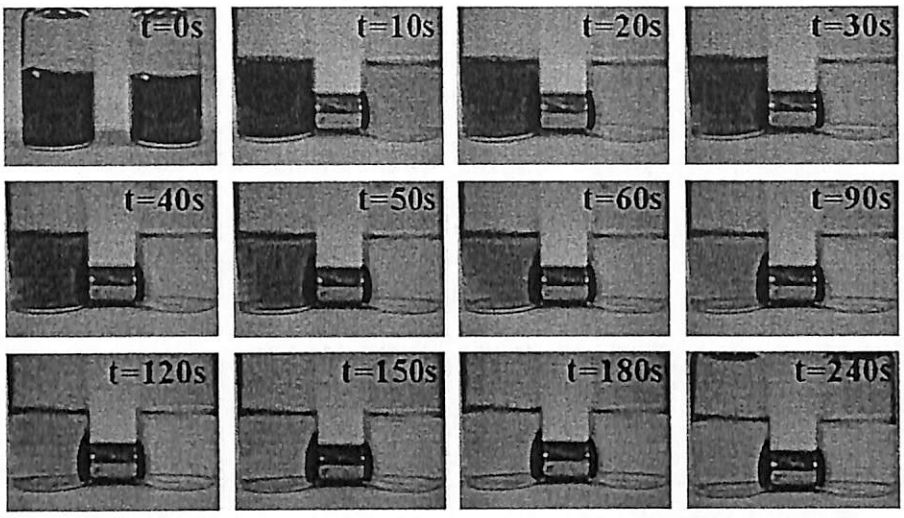

Fig. 5. Comparison the collection rate of (left) bare IOMNPs and (right) silica–PDDA–IOMNPs nanocomposite by a NdFeB magnet within 4 min. Both suspensions were prepared with concentration at 500 mg/L. The crystal clear solution formed at the end of magnetic collection for silica–PDDA–IOMNPs suspension also directly proved that both the silica colloid and IOMNPs have been integrated into one unified structure.

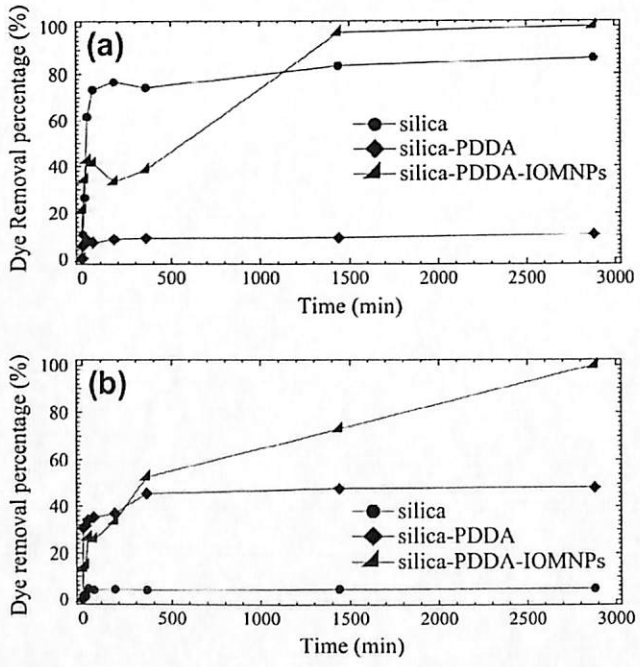

Fig. 6. Dye removal percentage of different as-synthesized nanoparticles used in (a) MB and (b) MO.

MB and MO removal by silica colloid suggested that electrostatic interaction plays an important role in dictating the adsorption-driven removal mechanism. Negatively charged silica colloids attracted and adsorbed positively charged MB but repelled MO with the same charge.

Silica colloids were then surface modified by the attachment of cationic PDDA. After the coating process, silica–PDDA turned out to be positively charged due to the outer PDDA shell formed on silica colloids. This highly charged silica–PDDA in turn can remove negatively charged MO (48.32%) (Fig. 6b and Fig. S1(f) in Supporting Information) better compared to MB (10.68%) (Fig. 6a and Fig. S1(d) in Supporting Information). Compared to the 86.64% removal of MB by oppositely charge silica colloids, there is only 48.32% removal of MO by silica–PDDA. We suspect that the underlying silica layer do play an important role in causing low percentage removal of MO by silica–PDDA structure. Even though there presents an extended layer of PDDA coating on the surface of silica colloid, as revealed by DLS measurement (see Table 1 for hydrodynamic diameter increment after PDDA attachment), this layer has limited capability to register oppositely charged MO into its matrix. The localized neutralization of charge after adsorption of MO onto PDDA layer(s) would cause the incoming MO to suffer higher resistant as the repulsion from underlying silica layer is more pronounced. This scenario is totally different from the case of MB adsorption onto bare silica colloid, in which the incoming MB can diffuse into mesoporous channel of silica and adsorbed on the inner surface of silica pore.

Apart from that, the removal of MB by silica–PDDA registered a none-zero value at 10.68% implied that, besides electrostatic, there is other interaction involved between MB and silica–PDDA even though they are both cationic. This observation lead us to believe hydrophobic interaction may also happened between hydrocarbon portion of dye molecule and non-polar part of PDDA [55]. Under this context, Seo and coworkers [56] discussed the contribution of electrostatic, hydrophobic and hydrogen bonding interaction on the sorption behavior of hydrogels and MO. In addition, Nandini and Vishalakshi [57] reported that reversal of metachromasy in MO-polyion complexes by adding alcohols/urea suggested the involvement of hydrophobic forces in polymer–dye interaction. As reported by both groups, the binding of dye molecules is primarily electrostatic force which is further reinforced by hydrophobic interaction. Therefore, the charge density and the flexibility of polyelectrolyte in terms of hydrophobicity of non-polar part and the bulkiness of the polar-part play vital role in polyelectrolyte–organic dye interaction. However, their work revealed that the electrostatic force is still the principal contributor to the dye removal. This is in consistent with our experiment results where the removal efficiency of MO (48.32%) is higher compared to MB (10.68%) by silica–PDDA.

Introduction of negatively charged IOMNPs into the positively charged silica–PDDA colloid has greatly suppressed the overall net surface charge of the final structure formed. At almost neutral pH, this silica–PDDA–IOMNPs nanocomposite exhibits a zeta potential value of +25.8 mV (as shown in Table 1). In this case, 100% removal of MB and MO was achieved by using silica–PDDA–IOMNPs nanocomposite (see Fig. 6) where at the end of the dye removal experiment, initial blue color of MB and orange

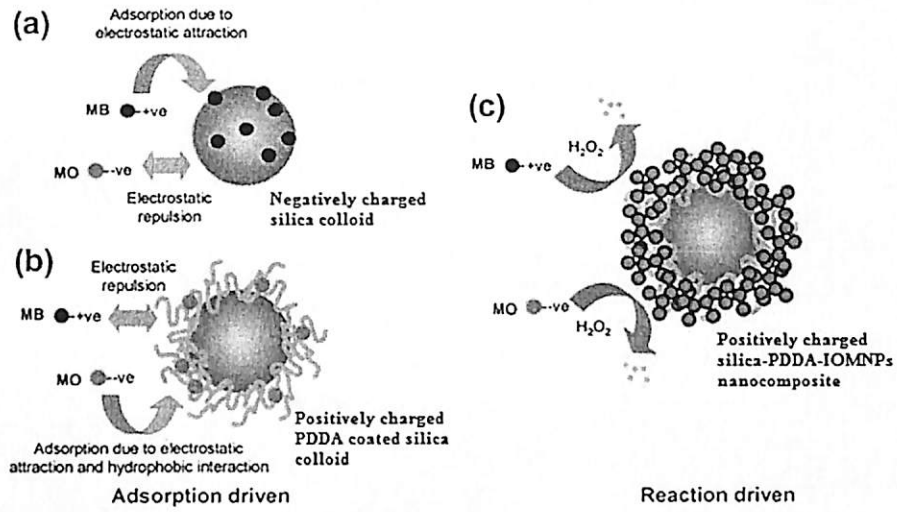

Fig. 7. Schematic diagram showing the electrostatic interactions and mechanisms involved for MB and MO removal by (a) silica colloid, (b) PDDA coated silica colloid, and (c) silica–PDDA–IOMNPs nanocomposite. For processes which are mainly driven by adsorption, such as (a) and (b), electrostatic play an important role in either promote or suppress the MB and MO removal depends on the charges of adsorbate (here dye molecules) and adsorbent (silica colloid and PDDA coated silica colloid). For silica–PDDA–IOMNPs nanocomposite, process (c), the influence of electrostatic interaction is negligible as Fenton-reaction dominating the removal mechanism.

color of MO will be completely decolorized. This scenario leads us to believe that both MB and MO have to be adsorbed onto silica–PDDA–IOMNPs nanocomposite, before Fenton reaction took place. According to Xue and coworkers, Fenton-like reaction is a surfaced-mediated process where the adsorption of H_2O_2 onto the surface of magnetite affected the whole reaction rate [58]. The proposed mechanisms required MB to be first adsorbed onto Fe_3O_4/FeM_nO_x before being decomposed by hydroxyl radical in a heterogeneous catalytic reaction [59]. At this point, the underlying mechanisms involved for the removal of both MB and MO by silica–PDDA–IOMNPs nanocomposite is unclear. However, it is quite certain that the dye molecules were adsorbed first before catalytically degraded via surface-mediated Fenton and Fenton-like reaction facilitated by IOMNPs within the nanocomposite. As a result, silica–PDDA–IOMNPs nanocomposite recorded the highest removal percentage for both MB and MO (see Fig. 6). This result also makes silica–PDDA–IOMNPs nanocomposite a superior candidate for water treatment purposes as its performance is independent of the charge of targeted pollutant.

From Fig. 8, it can be seen that without H_2O_2 (only dye and silica–PDDA–IOMNPs nanocomposite), dye removal by silica–PDDA–IOMNPs nanocomposite is significantly lower. In the presence of H_2O_2, both MB and MO were completely removed by silica–PDDA–IOMNPs nanocomposite of different loading. Higher silica–PDDA–IOMNPs nanocomposite loading leaded to faster degradation of dye components to achieve 100% removal efficiency. In consistent with Fig. S4 presented in the supporting document, we believe that the dominant mechanism for dyes removal of silica–PDDA–IOMNPs nanocomposite is catalytic degradation rather than adsorption. Nevertheless, adsorption does play a minor role as up to ~20% of dyes removal can still be achieved without the addition of H_2O_2 (see Fig. 8).

The lifespan of the as-synthesized silica–PDDA–IOMNPs nanocomposite was determined by repeating dye degradation for five runs with identical reaction conditions. To further ascertain the storage stability of the as-synthesized silica–PDDA–IOMNPs nanocomposite, the recycled dye degradation experiment was performed with the silica–PDDA–IOMNPs nanocomposite which have been stored for six months after its synthesis (see Fig. S4 in Supporting Information). Both MB and MO have been completely removed by the recycled silica–PDDA–IOMNPs nanocomposite.

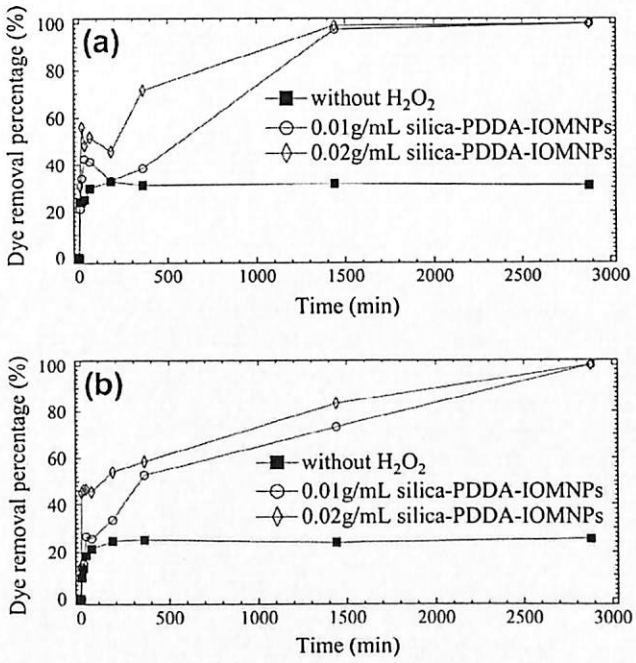

Fig. 8. Dye removal percentage of silica–PDDA–IOMNPs nanocomposite used in (a) MB and (b) MO.

This result implies that the silica–PDDA–IOMNPs nanocomposite has excellent reusability and can be used repeatedly for water treatment purposes.

3.3. MB and MO removal by adsorption

Adsorption isotherms are derived to relate the amount of solute adsorbed per unit mass of the adsorbent with the concentration of adsorbate in bulk solution at equilibrium condition. Although there are many well-established isotherms, none of them is found to be perfectly fitted the experimental data under all given conditions due to the complex nature of silica–PDDA–IOMNPs structure formed. Therefore, careful evaluation of adsorption isotherm is

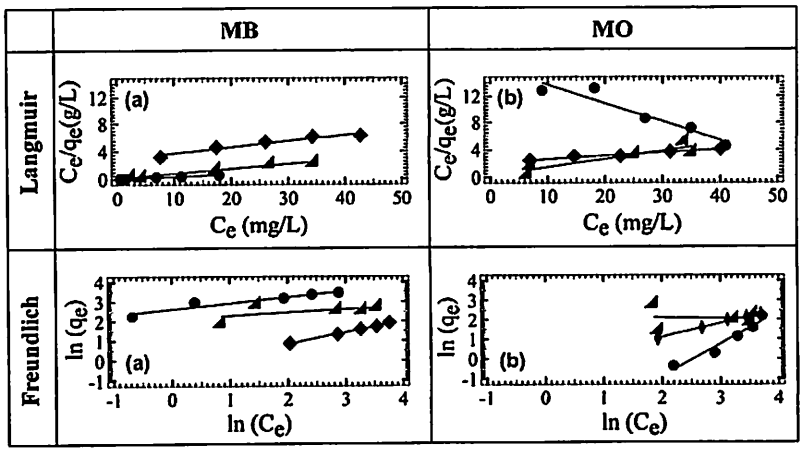

Fig. 9. Langmuir and Freundlich adsorption isotherm plots of (●) silica, (♦) silica–PDDA and (◢) silica–PDDA–IOMNPs nanocomposite in MB and MO dyes removal.

Table 2
Langmuir, Freundlich isotherm model constants with regression coefficient, separation factor, adsorption intensity and favorability.

		Langmuir							Freundlich				
		$q_{e,exp}$ (mg/g)	$q_{e,cal}$ (mg/g)	Q_o (mg/g)	b (L/mg)	R^2	R_L		$q_{e,cal}$ (mg/g)	K_F (mg/g (mg/L)$^{-1/n}$)	R^2	$1/n$	
Silica colloids	MB	31.68	31.56	32.47	0.86	0.99	0.023	Favor	42.28	14.49	0.92	0.29	Favor
	MO	9.00	7.26	−3.17	−0.017	0.91	6.29	Un-favor	6.79	0.016	0.95	1.63	Un-favor
Silica–PDDA	MB	6.83	6.37	11.38	0.031	0.94	0.39	Favor	6.40	0.69	0.99	0.60	Favor
	MO	9.81	9.75	20.79	0.022	0.92	0.48	Favor	10.47	0.61	0.99	0.77	Favor
Silica–PDDA–IOMNPs	MB	15.13	1.41	1.44	13.37	0.98	0.0010	Favor	7.57	4.85	0.57	0.35	Favor
	MO	9.87	5.12	8.39	0.44	0.83	0.043	Favor	6.03	4.92	0.13	0.16	Favor

needed based on (1) the relevancy of underlying assumptions, and (2) mathematically well fitted data. Langmuir and Freundlich model will be tested in this work as both of them have been widely used in solid–liquid adsorption system This analysis might not be physically valid due to the underlying assumption of both models but it does provide us a quantitative way to scrutinize the performance of silica–PDDA–IOMNPs nanocomposite in dye removal compared to just silica and silica–PDDA colloid.

Langmuir model assumed that monolayer coverage of adsorbate over a homogeneous adsorbent surface with energetically identical of all the adsorption sites and the isotherm is given as follow [60]:

$$q_e = \frac{Q_o b C_e}{1 + bC_e} \tag{3}$$

After linearization, Langmuir isotherm is in the form of equation as:

$$\frac{C_e}{q_e} = \frac{1}{bQ_o} + \frac{C_e}{Q_o} \tag{4}$$

where Q_o is a constant reflecting a complete monolayer (mg/g), b is adsorption equilibrium constant (L/mg) relating to the apparent energy of sorption, q_e is the equilibrium amount of solute adsorbed per unit weight of adsorbent (mg/g) and C_e is the equilibrium adsorbate concentration in solution (mg/L). In addition, equilibrium parameter R_L is used to express the essential characteristics of Langmuir isotherm. R_L is defined as follow [61]:

$$R_L = \frac{1}{1 + bC_o} \tag{5}$$

where C_o is the highest initial concentration of adsorbate (mg/L) used in adsorption isotherm study, and b (L/mg) is Langmuir constant. The value of R_L indicates the type of the Langmuir isotherm to be either unfavorable ($R_L > 1$), linear ($R_L = 1$), favorable ($0 < R_L < 1$), or irreversible ($R_L = 0$) [61]. By plotting Langmuir linear regression of C_e/q_e versus C_e shown in Fig. 9, the slope and intercept represented the $1/Q_o$ and $1/bQ_o$, respectively. The Langmuir equilibrium adsorption curves related the solid and liquid phase concentrations for dyes onto the as-synthesized nanoparticles [62].

On the other hand, Freundlich isotherm relates the liquid and solid phase capacity at equilibrium condition based on the multilayer adsorption takes place at heterogeneous surface by assuming that the adsorption sites are distributed exponentially with respect to the heat of adsorption and the equation is given as follow [63]:

$$q_e = K_F C_e^{1/n} \tag{6}$$

After linearization, Freundlich model in linear form is expressed as follow:

$$\ln(q_e) = \ln(K_F) + (1/n)\ln(C_e) \tag{7}$$

where K_F and n are Freundlich constants with K_F (mg/g (mg/L)$^{-1/n}$) is the multilayer adsorption capacity of the adsorbent and n is an empirical parameter related to the intensity of adsorption which varies with the heterogeneity of the adsorbent. A value in the range of $0.1 < 1/n < 1$ represents favorable adsorption condition [62]. Greater value of $1/n$ indicates that better is the favorability of the adsorption process [62]. By plotting $\ln(q_e)$ versus $\ln(C_e)$ shown in Fig. 9, the slope and intercept represented the $1/n$ and $\ln(K_F)$ respectively [62]. All isotherm parameters (Q_o, b, K_F, $1/n$) corresponding to Langmuir and Freundlich model together with regression coefficient, R^2 were summarized and compared in Table 2.

In the present study, for dyes removal by using silica colloids, the R_L for MB was 0.023 and for MO was 6.29, respectively, whereas the $1/n$ for MB and MO was 0.29 and 1.63. In both cases, the low R_L and $1/n$ values of MB indicated that the adsorption of MB onto the silica colloids is favorable whereas the adsorption of

Table 3
Comparison of the pseudo-first-order, pseudo-second-order adsorption rate constants and calculated and experimental q_e values with regression coefficient and nonlinear regression chi-square.

		Pseudo-first-order					Pseudo-second-order			
		$q_{e,exp}$ (mg/g)	$q_{e1,cal}$ (mg/g)	$k_1 \times 10^3$ (1/min)	R^2	χ^2	$q_{e2,cal}$ (mg/g)	$k_2 \times 10^3$ (g/mg/min)	R^2	$\chi^2 \times 10^5$
Silica colloids	MB	4.32	1.76	1.80	0.61	3.72	4.33	8.40	1.00	2.51
	MO	0.24	0.066	0.80	0.14	0.47	0.24	160.00	0.99	4.30
Silica–PDDA	MB	0.53	0.19	0.80	0.34	0.61	0.52	57.70	0.99	24.20
	MO	2.38	0.88	2.60	0.86	2.54	2.39	23.30	1.00	4.82
Silica–PDDA–IOMNPs	MB	4.95	4.13	2.30	0.94	0.16	5.14	1.26	0.96	756.00
	MO	5.33	4.33	0.80	0.90	0.23	5.28	1.12	0.97	53.60

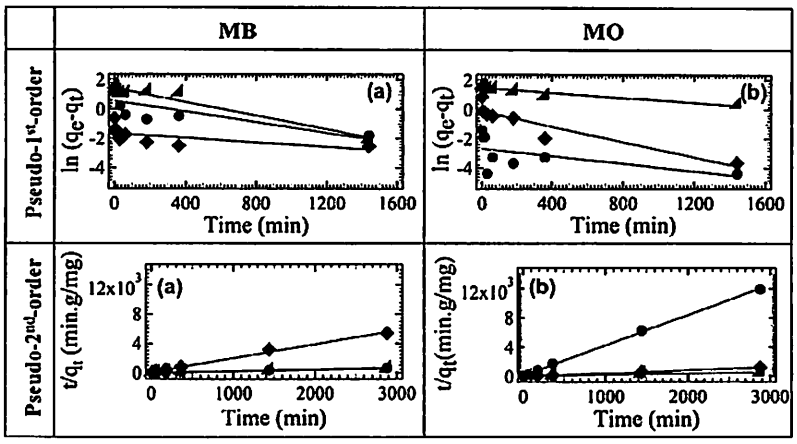

Fig. 10. Pseudo-first-order and pseudo-second-order kinetic plots of (●) silica, (♦) silica–PDDA and (◢) silica–PDDA–IOMNPs nanocomposite in MB and MO dyes removal.

MO onto silica colloids is completely unfavorable. This observation provided indirect hint that the electrostatic interaction played the major role for negatively charged silica colloids to remove oppositely charged MB instead of MO with same charge. In MB removal by silica colloids, higher R^2 was obtained from Langmuir isotherm compared to Freundlich isotherm reflected that the adsorption of MB on silica colloids can be explained via Langmuir model. This is consistent with the underlying assumption of Langmuir isotherm [60] suggesting that once the MB molecule occupies a site on silica surface, no further adsorption can take place at the occupied site due to electrostatic repulsion.

In second stage, silica–PDDA nanoparticles were employed in dyes removal test where the R_L for MB and MO was 0.39 and 0.48 respectively and $1/n$ for MB and MO was 0.60 and 0.77 showing that the adsorption of both MB and MO was favorable on silica–PDDA. However, higher $1/n$ value for MO indicated that the MO was more favorable to the electrostatic driven entrapment (Fig. 7b) of oppositely charged MB into PDDA open matrix. Higher R^2 of MB and MO in Freundlich compared to Langmuir isotherm indicated that the adsorption of both dyes by silica–PDDA at equilibrium can be described using Freundlich isotherm model. This finding is consistent with the fact that the silica–PDDA colloids surface is more heterogeneous with the extension of polyelectrolyte layers allow the multilayer adsorption of dye molecules.

The R_L values for both MB and MO in dyes removal test of silica–PDDA–IOMNPs nanocomposite were 0.0010 and 0.043, respectively. Whereas $1/n$ values for MB and MO were 0.35 and 0.16. These results indicated that the adsorption of both MB and MO was favorable. Moreover, R^2 from curve fitting of both dyes removal by silica–PDDA–IOMNPs nanocomposite registered higher values for Langmuir model. This result showed that the adsorption of both dyes by silica–PDDA–IOMNPs nanocomposite in time constraint can be illustrated better using Langmuir theory where the dyes were adsorbed with equal activation energy as monolayer onto homogeneous silica–PDDA–IOMNPs nanocomposite surface. This puzzling observation should be related to the time scale for adsorption and catalytic degradation to happen. We suspect the catalytic degradation of dye molecules by IOMNPs prohibits the multilayer adsorption as observed in silica–PDDA system.

3.4. MB and MO removal by reaction

In this work two kinetic models, namely pseudo-first-order and pseudo-second-order, were used to fit the kinetic data. The equations are formulated by considering the driving force of removal is proportional to the difference of dye removed by nanoparticles at each time steps prior to equilibrium condition.

Pseudo-first and pseudo-second kinetic models for the dye removal from aqueous solution are written as follow [64]:

$$\frac{dq_t}{dt} = k_1(q_e - q_t) \tag{8}$$

$$\frac{dq_t}{dt} = k_2(q_e - q_t)^2 \tag{9}$$

where q_e and q_t are the amounts of solute (mg/g) per unit of dye removal agent at equilibrium and at time t, respectively. k_1 is the pseudo-first-order rate constant (1/min) and k_2 is the pseudo-second-order rate constant (g/mg/min). After integration by applying the initial conditions $q_t = 0$ at $t = 0$ and $q_t = q_t$ at $t = t$, a linear form of pseudo-first-order and pseudo-second-order models are shown as below [64]:

$$\ln(q_e - q_t) = \ln(q_e) - k_1 t \tag{10}$$

$$\frac{t}{q_t} = \frac{1}{k_2 q_e^2} + \frac{t}{q_e} \quad (11)$$

In this manner, kinetic model is evaluated by analyzing the correlation coefficient (R^2) and nonlinear regression chi-square (χ^2) obtained from the curve fittings.

The values of the calculated and experimental of q_e and rate constants k_1 and k_2 determined from the models are presented in Table 3 along with the correlation coefficient (R^2) and nonlinear regression chi-square (χ^2).

Comparing kinetic plots of pseudo-first-order and pseudo-second-order in Fig. 10, good linearization of the experimental data was observed for pseudo-second-order kinetic plots. It can be seen from Table 3, all values of R^2 were closer to unity for pseudo-second-order model than the pseudo-first-order model. Furthermore, the calculated equilibrium adsorption capacity values, $q_{e2,cal}$ from pseudo-second-order equation were much closer to the experimental values, $q_{e,exp}$ and this was confirmed by the lower values of nonlinear regression chi-square (χ^2). Thereby, the results implied that the rate of dye removal by the synthesized nanocomposite followed pseudo-second-order kinetic model. It is worth mentioning that the pseudo-second-order equation is more widely applicable than pseudo-first-order equation to most of the studied system because the sorption capacity, rate constant of pseudo-second-order as well as the initial removal rate can be determined from the equation without any prior knowledge on the parameters involved [65]. Therefore, as organic dye removal by Fe-based hybrid material is concerned, the associated kinetic is better represented by pseudo-second-order model such as those observed in the MB and MO removal by green tea leaf-iron nanoparticles [37], MB removal by perlite [66] and montmorillonite/$CoFe_2O_4$ composite [67] as well as MO removal by maghemite/chitosan nanocomposite films [68] and activated carbon/Fe_3O_4 nanoparticle composite [69].

4. Conclusion

Iron oxide magnetic nanoparticles decorated silica colloid can be synthesized through layer-by-layer assembly with PDDA as binding agent. At each stage of synthesis, due to charge reversal, the nanostructure formed could remove oppositely charged dye molecules. For simple silica colloid system, electrostatic interaction is the sole contributor in dictating the removal of MB. After surface functionalized by PDDA polyelectrolyte, the silica–PDDA structure formed is more effective in removing MO than MB. Under this scenario, in addition to electrostatic driven adsorption, we believe that hydrophobic interaction plays an important role for the full functioning of silica–PDDA particles. The presence of hydrophobic interaction between the dye molecule and non-polar segment of PDDA is also the main reason for silica–PDDA particles to be capable of removing MB even though there is obvious electrostatic repulsion between them. The final silica–PDDA–IOMNPs nanocomposite formed has exhibit magnetic and catalytic dual functionalities. This nanocomposite can be magnetophoretically collected by a permanent magnet at much rapid rate (<1 min) compared to the IOMNPs at same concentration. For dye removal, silica–PDDA–IOMNPs nanocomposite has recorded a dye removal efficiency of ~100% neglecting the charge of dye involved. This nanocomposite is a much versatile nanoagent for environmental engineering application and can be repeatedly used for at least 5 times for water treatment purpose and remained to be catalytically active after 6 months. The adsorption isotherm data for silica–PDDA–IOMNPs nanocomposite in dye removal were well fitted with Langmuir model suggested that the adsorption occurred with monolayer coverage before Fenton and Fenton-like reaction took place to catalytically degrade the adsorbed MB and MO dyes. Dye removal kinetic of this nanocomposite which involves electrostatic interaction on adsorption process and further catalytic degradation mechanism was described appropriately by pseudo-second-order kinetic model.

Acknowledgments

This project is financially supported by RU Grant from Universiti Sains Malaysia (Grant No. 1001/PJKIMIA/811219), Exploratory Research Grants Scheme (ERGS) with (Grant No. 203/PJKIMIA/6730012) and International Foundation for Science (IFS) (Grant No. 304/PJKIMIA/6050232). All authors are affiliated to Membrane Science and Technology Cluster of USM.

Appendix A. Supplementary material

Fig. S1: Images of silica, silica–PDDA, and removal of MB and MO by silica and silica–PDDA respectively. Fig. S2: Magnetophoretic collective rate of silica–PDDA–IOMNPs nanocomposite before and after usage. Fig. S3: Colloidal stability profile of silica–PDDA–IOMNPs and bare IOMNPs in electrolyte condition. Fig. S4: Removal of MB (a) and MO (b) by using 6 months old silica–PDDA–IOMNPs comparing with silica in MB removal and silica–PDDA in MO removal respectively. Supplementary data associated with this article can be found, in the online version, at http://dx.doi.org/10.1016/j.cej.2013.12.095.

References

[1] Q.A. Pankhurst, N.T.K. Thanh, S.K. Jones, J. Dobson, Progress in applications of magnetic nanoparticles in biomedicine, J. Phys. D Appl. Phys. 42 (2009) 224001.
[2] N.L. Adolphi, D.L. Huber, H.C. Bryant, T.C. Monson, D.L. Fegan, J. Lim, J.E. Trujillo, T.E. Tessier, D.M. Lovato, K.S. Butler, P.P. Provencio, H.J. Hathaway, S.A. Majetich, R.S. Larson, E.R. Flynn, Characterization of single-core magnetite nanoparticles for magnetic imaging by SQUID relaxometry, Phys. Med. Biol. 55 (2010) 5985.
[3] K.E. McCloskey, J.J. Chalmers, M. Zborowski, Magnetic cell separation: characterization of magnetophoretic mobility, Anal. Chem. 75 (2003) 6868–6874.
[4] P.Y. Toh, S.P. Yeap, L.P. Kong, B.W. Ng, D.J.C. Chan, A.L. Ahmad, J.K. Lim, Magnetophoretic removal of microalgae from fishpond water: feasibility of high gradient and low gradient magnetic separation, Chem. Eng. J. 211–212 (2012) 22–30.
[5] B. Saha, S. Das, J. Saikia, G. Das, Preferential and enhanced adsorption of different dyes on iron oxide nanoparticles: a comparative study, J. Phys. Chem. C. 115 (2011) 8024–8033.
[6] C.T. Yavuz, J.T. Mayo, W.W. Yu, A. Prakash, J.C. Falkner, S. Yean, L. Cong, H.J. Shipley, A. Kan, M. Tomson, D. Natelson, V.L. Colvin, Low-field magnetic separation of monodisperse Fe_3O_4 nanocrystals, Science 314 (2006) 964–967.
[7] J. Hu, G. Chen, I.M.C. Lo, Removal and recovery of Cr(VI) from wastewater by maghemite nanoparticles, Water Res. 39 (2005) 4528–4536.
[8] A.C. Balazs, T. Emrick, T.P. Russell, Nanoparticle polymer composites: where two small worlds meet, Science 314 (2006) 1107–1110.
[9] T.R. Pisanic II, J.D. Blackwell, V.I. Shubayev, R.R. Fiñones, S. Jin, Nanotoxicity of iron oxide nanoparticle internalization in growing neurons, Biomaterials 28 (2007) 2572–2581.
[10] P. Yuan, D. Liu, M. Fan, D. Yang, R. Zhu, F. Ge, J. Zhu, H. He, Removal of hexavalent chromium [Cr(VI)] from aqueous solutions by the diatomite-supported/unsupported magnetite nanoparticles, J. Hazard. Mater. 173 (2010) 614–621.
[11] M.H. Sousa, J.C. Rubim, P.G. Sobrinho, F.A. Tourinho, Biocompatible magnetic fluid precursors based on aspartic and glutamic acid modified maghemite nanostructures, J. Magn. Magn. Mater. 225 (2001) 67–72.
[12] S.P. Yeap, A.L. Ahmad, B.S. Ooi, J. Lim, Electrosteric stabilization and its role in cooperative magnetophoresis of colloidal magnetic nanoparticles, Langmuir 28 (2012) 14878–14891.
[13] A.L.-T. Pham, C. Lee, F.M. Doyle, D.L. Sedlak, A silica-supported iron oxide catalyst capable of activating hydrogen peroxide at neutral pH values, Environ. Sci. Technol. 43 (2009) 8930–8935.
[14] M. Mandal, S. Kundu, S.K. Ghosh, S. Panigrahi, T.K. Sau, S.M. Yusuf, T. Pal, Magnetite nanoparticles with tunable gold or silver shell, J. Colloid Interface Sci. 286 (2005) 187–194.
[15] L.P. Kong, X.J. Gan, A.L.B. Ahmad, B.H. Hamed, E.R. Evarts, B.S. Ooi, J. Lim, Design and synthesis of magnetic nanoparticles augmented microcapsule with catalytic and magnetic bifunctionalities for dye removal, Chem. Eng. J. 197 (2012) 350–358.

[16] Y. Liu, A. Wang, R.O. Claus, Layer-by-layer electrostatic self-assembly of nanoscale Fe3O4 particles and polyimide precursor on silicon and silica surfaces, Applied Physics Letters. 71 (1997) 2265–2267.
[17] W. Tan, K. Wang, X. He, X.J. Zhao, T. Drake, L. Wang, R.P. Bagwe, Bionanotechnology based on silica nanoparticles, Med. Res. Rev. 24 (2004) 621–638.
[18] M.N. Ahmed, R.N. Ram, Removal of basic dye from waste-water using silica as adsorbent, Environ. Pollut. 77 (1992) 79–86.
[19] G. McKay, M.S. Otterburn, A.G. Sweeney, Surface mass transfer processes during colour removal from effluent using silica, Water Res. 15 (1981) 327–331.
[20] X. Zhao, Y. Shi, T. Wang, Y. Cai, G. Jiang, Preparation of silica-magnetite nanoparticle mixed hemimicelle sorbents for extraction of several typical phenolic compounds from environmental water samples, J. Chromatogr. A 1188 (2008) 140–147.
[21] K. Hofstadler, R. Bauer, S. Novalic, G. Heisler, New reactor design for photocatalytic wastewater treatment with TiO_2 immobilized on fused-silica glass fibers: photomineralization of 4-chlorophenol, Environ. Sci. Technol. 28 (1994) 670–674.
[22] N.M. Mahmoodi, S. Khorramfar, F. Najafi, Amine-functionalized silica nanoparticle: preparation, characterization and anionic dye removal ability, Desalination 279 (2011) 61–68.
[23] M. Ohmori, E. Matijević, Preparation and properties of uniform coated colloidal particles. VII. Silica on hematite, J. Colloid Interface Sci. 150 (1992) 594–598.
[24] A.P. Philipse, M.P.B. van Bruggen, C. Pathmamanoharan, Magnetic silica dispersions: preparation and stability of surface-modified silica particles with a magnetic core, Langmuir 10 (1994) 92–99.
[25] P. Tartaj, T. González-Carreño, C.J. Serna, Magnetic behavior of γ-Fe_2O_3 nanocrystals dispersed in colloidal silica particles, J. Phys. Chem. B 107 (2002) 20–24.
[26] H. Matsumoto, D. Nagao, M. Konno, Repetitive heterocoagulation of oppositely charged particles for enhancement of magnetic nanoparticle loading into monodisperse silica particles, Langmuir 26 (2009) 4207–4211.
[27] Y. Zhu, H. Da, X. Yang, Y. Hu, Preparation and characterization of core–shell monodispersed magnetic silica microspheres, Colloids Surf., A 231 (2003) 123–129.
[28] M. Benelmekki, C. Caparros, A. Montras, R. Gonçalves, S. Lanceros-Mendez, L.M. Martinez, Horizontal low gradient magnetophoresis behaviour of iron oxide nanoclusters at the different steps of the synthesis route, J. Nanopart. Res. 13 (2011) 3199–3206.
[29] J. Faraudo, J. Camacho, Cooperative magnetophoresis of superparamagnetic colloids: theoretical aspects, Colloid Polym. Sci. 288 (2010) 207–215.
[30] J. Lim, C. Lanni, E.R. Evarts, F. Lanni, R.D. Tilton, S.A. Majetich, Magnetophoresis of nanoparticles, ACS Nano 5 (2010) 217–226.
[31] J.K. Lim, S.A. Majetich, R.D. Tilton, Stabilization of superparamagnetic iron oxide core–gold shell nanoparticles in high ionic strength media, Langmuir 25 (2009) 13384–13393.
[32] S.P. Yeap, P.Y. Toh, A.L. Ahmad, S.C. Low, S.A. Majetich, J. Lim, Colloidal stability and magnetophoresis of gold-coated iron oxide nanorods in biological media, J. Phys. Chem. C 116 (2012) 22561–22569.
[33] M. Auffan, J. Rose, J.Y. Bottero, G.V. Lowry, J.P. Jolivet, M.R. Wiesner, Towards a definition of inorganic nanoparticles from an environmental, health and safety perspective, Nat. Nanotechnol. 4 (2009) 634–641.
[34] H. Wang, Y. Huang, Prussian-blue-modified iron oxide magnetic nanoparticles as effective peroxidase-like catalysts to degrade Methylene Blue with H_2O_2, J. Hazard. Mater. 191 (2011) 163–169.
[35] A. Mittal, A. Malviya, D. Kaur, J. Mittal, L. Kurup, Studies on the adsorption kinetics and isotherms for the removal and recovery of Methyl Orange from wastewaters using waste materials, J. Hazard. Mater. 148 (2007) 229–240.
[36] R. Andreozzi, V. Caprio, A. Insola, R. Marotta, Advanced oxidation processes (AOP) for water purification and recovery, Catal. Today 53 (1999) 51–59.
[37] T. Shahwan, S. Abu Sirriah, M. Nairat, E. Boyacı, A.E. Eroğlu, T.B. Scott, K.R. Hallam, Green synthesis of iron nanoparticles and their application as a Fenton-like catalyst for the degradation of aqueous cationic and anionic dyes, Chem. Eng. J. 172 (2011) 258–266.
[38] F. Ji, C. Li, J. Zhang, L. Deng, Efficient decolorization of dye pollutants with LiFe(WO4)2 as a reusable heterogeneous Fenton-like catalyst, Desalination 269 (2011) 284–290.
[39] W. Luo, L. Zhu, N. Wang, H. Tang, M. Cao, Y. She, Efficient removal of organic pollutants with magnetic nanoscaled $BiFeO_3$ as a reusable heterogeneous fenton-like catalyst, Environ. Sci. Technol. 44 (2010) 1786–1791.
[40] F.C.C. Moura, M.H. Araujo, R.C.C. Costa, J.D. Fabris, J.D. Ardisson, W.A.A. Macedo, R.M. Lago, Efficient use of Fe metal as an electron transfer agent in a heterogeneous Fenton system based on Fe0/Fe_3O_4 composites, Chemosphere 60 (2005) 1118–1123.
[41] S.H. Joo, A.J. Feitz, T.D. Waite, Oxidative degradation of the carbothioate herbicide, molinate, using nanoscale zero-valent iron, Environ. Sci. Technol. 38 (2004) 2242–2247.
[42] V. Kitsiou, N. Filippidis, D. Mantzavinos, I. Poulios, Heterogeneous and homogeneous photocatalytic degradation of the insecticide imidacloprid in aqueous solutions, Appl. Catal. B 86 (2009) 27–35.
[43] O.B. Ayodele, J.K. Lim, B.H. Hameed, Pillared montmorillonite supported ferric oxalate as heterogeneous photo-Fenton catalyst for degradation of amoxicillin, Appl. Catal. A 413–414 (2012) 301–309.
[44] E. Elmolla, M. Chaudhuri, Optimization of Fenton process for treatment of amoxicillin, ampicillin and cloxacillin antibiotics in aqueous solution, J. Hazard. Mater. 170 (2009) 666–672.
[45] T. Phenrat, N. Saleh, K. Sirk, R.D. Tilton, G.V. Lowry, Aggregation and sedimentation of aqueous nanoscale zerovalent iron dispersions, Environ. Sci. Technol. 41 (2006) 284–290.
[46] W.G. Kuo, Decolorizing dye wastewater with Fenton's reagent, Water Res. 26 (1992) 881–886.
[47] J. Fernandez, J. Bandara, A. Lopez, P. Buffat, J. Kiwi, Photoassisted Fenton degradation of nonbiodegradable azo dye (Orange II) in Fe-free solutions mediated by cation transfer membranes, Langmuir 15 (1998) 185–192.
[48] F. Carnal, S. Stoll, Adsorption of weak polyelectrolytes on charged nanoparticles, impact of salt valency, pH, and nanoparticle charge density. Monte Carlo simulations, J. Phys. Chem. B 115 (2011) 12007–12018.
[49] P. Deo, N. Deo, P. Somasundaran, S. Jockusch, N.J. Turro, Conformational changes of pyrene-labeled polyelectrolytes with ph: effect of hydrophobic modifications, J. Phys. Chem. B 109 (2005) 20714–20718.
[50] M. Baalousha, A. Manciulea, S. Cumberland, K. Kendall, J.R. Lead, Aggregation and surface properties of iron oxide nanoparticles: Influence of ph and natural organic matter, Environ. Toxicol. Chem. 27 (2008) 1875–1882.
[51] F. Gazeau, J.C. Bacri, F. Gendron, R. Perzynski, Y.L. Raikher, V.I. Stepanov, E. Dubois, Magnetic resonance of ferrite nanoparticles: evidence of surface effects, J. Magn. Magn. Mater. 186 (1998) 175–187.
[52] N. Saleh, H.-J. Kim, T. Phenrat, K. Matyjaszewski, R.D. Tilton, G.V. Lowry, Ionic strength and composition affect the mobility of surface-modified Fe0 nanoparticles in water-saturated sand columns, Environ. Sci. Technol. 42 (2008) 3349–3355.
[53] G.J. Fleer, Polymers at interfaces and in colloidal dispersions, Adv. Colloid Interface Sci. 159 (2010) 99–116.
[54] G.J. Fleer, J.M.H.M. Scheutjens, M.A.C. Stuart, Theoretical progress in polymer adsorption, steric stabilization and flocculation, Colloids Surf. 31 (1988) 1–29.
[55] T. Takagishi, K. Nakagami, K. Imajo, N. Kuroki, Interaction of poly(vinylpyrrolidone) with Methyl Orange and its homologs in aqueous solution over the temperature range 60–90 °C, J. Polym. Sci.: Polym. Chem. Ed. 14 (1976) 923–929.
[56] T. Seo, S. Hagura, T. Kanbara, T. Iijima, Interaction of dyes with chitosan derivatives, J. Appl. Polym. Sci. 37 (1989) 3011–3027.
[57] R. Nandini, B. Vishalakshi, A study of interaction of Methyl Orange with some polycations, E-Journal Chem. 9 (2012) 1–14.
[58] X. Xue, K. Hanna, M. Abdelmoula, N. Deng, Adsorption and oxidation of PCP on the surface of magnetite: Kinetic experiments and spectroscopic investigations, Appl. Catal. B 89 (2009) 432–440.
[59] S. Xing, Z. Zhou, Z. Ma, Y. Wu, Characterization and reactivity of Fe_3O_4/FeMnOx core/shell nanoparticles for Methylene Blue discoloration with H_2O_2, Appl. Catal. B 107 (2011) 386–392.
[60] I. Langmuir, The adsorption of gases on plane surfaces of glass, mica and platinum, J. Am. Chem. Soc. 40 (1918) 1361–1403.
[61] T.W. Webi, R.K. Chakravort, Pore and solid diffusion models for fixed-bed adsorbers, AIChE J. 20 (1974) 228–238.
[62] B.H. Hameed, D.K. Mahmoud, A.L. Ahmad, Equilibrium modeling and kinetic studies on the adsorption of basic dye by a low-cost adsorbent: coconut (Cocos nucifera) bunch waste, J. Hazard. Mater. 158 (2008) 65–72.
[63] H. Freundlich, U. Leipzig, Über die Absorption in Lösungen, Universität Leipzig, 1906.
[64] S. Lagergren, About the theory of so called adsorption of soluble substances, Kungliga Svenska Vetenskapsakademiens. Handlinglar, Band 24. (1898) 1–6.
[65] Y.S. Ho, G. McKay, Pseudo-second order model for sorption processes, Process Biochem. 34 (1999) 451–465.
[66] M. Doğan, M. Alkan, A. Türkyilmaz, Y. Özdemir, Kinetics and mechanism of removal of Methylene Blue by adsorption onto perlite, J. Hazard. Mater. 109 (2004) 141–148.
[67] L. Ai, Y. Zhou, J. Jiang, Removal of Methylene Blue from aqueous solution by montmorillonite/$CoFe_2O_4$ composite with magnetic separation performance, Desalination 266 (2011) 72–77.
[68] R. Jiang, Y.-Q. Fu, H.-Y. Zhu, J. Yao, L. Xiao, Removal of Methyl Orange from aqueous solutions by magnetic maghemite/chitosan nanocomposite films: adsorption kinetics and equilibrium, J. Appl. Polym. Sci. 125 (2012) E540–E549.
[69] M.H. Do, N.H. Phan, T.D. Nguyen, T.T.S. Pham, V.K. Nguyen, T.T.T. Vu, T.K.P. Nguyen, Activated carbon/Fe_3O_4 nanoparticle composite: Fabrication, Methyl Orange removal and regeneration by hydrogen peroxide, Chemosphere 85 (2011) 1269–1276.